UNIVERSITY OF SÃO PAULO

DEPARTMENT OF MECHANICAL ENGINEERING

EDUARDO AGUIAR MENDES

Topology optimization for stability problems of submerged structures using the TOBS method

Santos

2022

EDUARDO AGUIAR MENDES

Topology optimization for stability problems of submerged structures using the TOBS method

Revised version

Master thesis presented to the Graduate Program in Mechanical Engineering at the Department of Mechanical Engineering (PME), Polytechnic School of University of São Paulo (EPUSP), to obtain the degree of Master of Science.

Concentration area: Mechanical Engineering of Design and Manufacturing

Advisor: **Dr. Renato Picelli**
Young Investigator FAPESP [2018/05797-8]

Santos

2022

Este exemplar foi revisado e corrigido em relação à versão original, sob responsabilidade única do autor e com a anuência de seu orientador.

São Paulo, __13__ de ___Janeiro_____ de ___2022_____

Assinatura do autor: _____

Assinatura do orientador: _____

Catalogação-na-publicação

Dedicatória

Aos meus amados pais, Arlete e Sebastião, e à minha querida irmã, Priscila, sem os quais não sou nada.

Agradecimentos

A Deus, por me permitir viver em plenitude todas as bênçãos que recebi e hei de receber em minha vida.

Aos meus pais, Arlete e Sebastião, que me proporcionaram em cada momento de vida as melhores condições para ser quem sou e chegar aonde gostaria, e à minha irmã, Priscila, que me ensinou o significado de parceria e amor incondicional. Sou imensamente grato e lhes dedico cada sonho que conquistei e ainda irei conquistar.

Ao meu orientador Renato Picelli, que soube compartilhar um imenso conhecimento nesses anos por meio de uma didática serena, paciente e inspiradora. Um exemplo de pesquisador, professor e amigo que levarei para a vida.

Aos meus amigos, de incontáveis anos aos recém chegados, que apesar da distância física puderam se fazer presentes em coração e serem valiosas fontes de afeto, parceria e momentos de alegria. O mundo não teria a graça de ser vivenciado sem as amizades que carrego.

Aos professores e colegas da Universidade de São Paulo, que foram imprescindíveis para meu crescimento acadêmico e pessoal em tempos desafiadores. Aos parceiros de LASG, pela oportunidade de compartilhar momentos descontraídos e memoráveis em meio à tentativa de colaborar para a ciência brasileira. Aos professores Ronaldo Carrion e Rafael Gioria, pelas experiências em sala de aula, orientações fundamentais e fonte de sabedoria transmitidas de um maneira tão humilde e inspiradora. Ao Professor René Quispe, que foi fundamental para a minha trajetória na pesquisa desde a graduação, e se tornou referência em minha vida profissional e ética.

Acknowledgements

Resumo

MENDES, E. A. **Otimização topológica para problemas de estabilidade de estruturas submersas utilizando o método TOBS**. 2021. Dissertação (Mestrado). Escola Politécnica da Universidade de São Paulo, São Paulo, Brasil.

A otimização estrutural topológica tem se difundido cada vez mais nos meios acadêmico e industrial em função de sua maior liberdade de projeto e a disponibilidade crescente de poder computacional. Típicos problemas de Otimização Topológica (OT) buscam a maximização da rigidez de estruturas com restrição de volume por meio de métodos baseados em densidades, podendo gerar soluções com desempenho insatisfatório de estabilidade, como, por exemplo, estruturas propensas à flambagem. Uma alternativa válida propõe implementar o parâmetro de flambagem no problema de otimização como restrição, obtendo soluções finais que já satisfazem esse critério. Nesse contexto, os métodos binários - que geram apenas designs com sólidos 1 e vazios 0 - se inserem como uma abordagem eficiente na solução de problemas de otimização, em especial os multifísicos, cuja precisa definição de fronteira estrutural é essencial. Uma aplicação desafiadora para problemas de OT que se beneficia dessa classe de método são as estruturas submersas, como os componentes da indústria *offshore*, sujeitos a cargas dependentes do *design* e que podem apresentar problemas de estabilidade. Esse tipo de carregamento impõe uma mudança constante do local, direção e magnitude do carregamento do fluido, o que não é tido como trivial em procedimentos de otimização. Nesse cenário, o objetivo desse trabalho é investigar a natureza binária do método TOBS por meio da solução de problemas de otimização topológica que consideram restrições de flambagem e cargas dependentes do *design*, características de sistemas estruturais submersos. O problema de otimização topológica proposto ainda não foi explorado na literatura. A implementação de flambagem linear foi verificada por meio de métodos analíticos, e um problema de otimização com restrição de flambagem de referência foi resolvido para garantia de sua eficência. Exemplos numéricos de estruturas sob carregamento de pressão foram otimizados e investigados quanto à influência do parâmetro de estabilidade quando comparados às soluções clássicas de minimização de *compliance*. Discussões sobre os problemas comuns associados à equação de autovalor e autovetor que rege o fenômeno de flambagem linear, bem como os parâmetros adotados no método do TOBS, foram apresentadas. A configuração binária proposta demonstrou resultados promissores ao obter soluções finais com melhoria significativa na resistência à flambagem e mínima perda de rigidez. Estudos de tempo computacional mostraram que as sensibilidades de flambagem são o gargalo do processo de otimização e, portanto, técnicas alternativas para lidar com esse parâmetro devem ser investigadas.

Palavras-chave: Otimização topológica. Restrição de flambagem. Variáveis binárias. Carregamento de pressão.

Abstract

MENDES, E. A. **Topology optimization for stability problems of submerged structures using the TOBS method**. 2021. Thesis (Masters). Escola Politécnica of the University of São Paulo, São Paulo, Brazil.

Structural topology optimization is increasingly used across academia and industry because of the great design freedom it offers and due to the rising computational power availability. Typical Topology Optimization (TO) problems seek stiffness maximization for volume-constrained structures via density-based methods, which may generate solutions with poor stability performance, e.g. prone to buckling. A valid alternative is to include the buckling parameter as a constraint in order to obtain final designs that fulfill this criterion. In this context, binary methods - which generates clear [0,1] designs - emerge as an effective approach to solve multiphysics problems, wherein precise definition of the structural boundary is essential. A challenging TO application that benefits from this class of methods are submerged structures, e.g. offshore industry components, which are subject to design-dependent loads and might present stability issues. This loading type imposes a constant change on fluid loading location, direction and magnitude, which is not trivial for optimization procedures. In this scenario, the aim of this work it to investigate the binary nature of the TOBS method by solving topology optimization problems that consider buckling constraints and design-dependent loads, characteristic of submerged structural systems. The proposed topology optimization problem has not been explored in the literature. The linear buckling implementation is verified through analytical methods, and a benchmark optimization problem for buckling-constrained formulation is solved for efficiency analysis. Numerical examples of pressure-loaded structures are optimized and investigated regarding the stability parameter effect when compared to classic compliance minimization solutions. Further discussions are held concerning the common issues associated with the buckling eigenproblem, as well as the main parameters adopted in the TOBS method. The proposed binary framework presented promising results by obtaining final solutions with significant improvement in buckling resistance and minimal stiffness loss when compared to the compliance designs. Computational time studies showed that the buckling sensitivities are the bottleneck of the optimization process and, thus, alternative techniques should be investigated.

Keywords: Topology optimization. Buckling constraints. Binary variables. Pressure loading.

List of Figures

Nomenclature

Latin Letters

$\mathbf{B}$ Matrix with derivatives of the finite element shape functions

c Level set function value that defines the structural interface

$C(\mathbf{x})$ Structural mean compliance

D Critical buckling load factor difference parameter

$\mathbf{D}$ Elasticity matrix

E Young's modulus

$f(\mathbf{x})$ Objective function

$\mathbf{f}_{fs}$ Global vector of interface fluid to structure forces

$\mathbf{F}$ General vector of nodal loads

F_{cr} Critical buckling load

F_0 Reference load

$g(\mathbf{x})$ Inequality constraint

$\overline{g}$ Inequality constraint upper limit

$\mathbf{G}$ Shape function derivatives matrix

H_{jm} Weight factor for filtering

$h(\mathbf{x})$ Equality constraint

I Minimum moment of inertia for the column's cross-sectional area

j Finite element

k Iteration number

K Set of critical buckling modes to eigevalue multiplicity

$\mathbf{K}$ General global stiffness matrix

$\mathbf{K}_s$ Global structural stiffness matrix

$\mathbf{K}_f$ Global fluid stiffness matrix

$\mathbf{K}_\sigma$ General global stress stiffness matrix

L Column length

$\mathbf{L}_{fs}$ Spatial fluid-structure coupling matrix

$\mathbf{L}_{fs}^*$ Spatial fluid-structure coupling matrix after an element removal

M Set of computed buckling modes

m Elements whose center-to-center distance is smaller than r

$\mathbf{n}$ Normal vector

N_e Number of equality constraints

N_d Number of design variables

N_g Number of inequality constraints

N_m Set of elements m

$\mathbf{N}_s$ Finite element shape functions for the structure

$\mathbf{N}_f$ Finite element shape functions for the fluid

p Penalty factor

$\mathbf{P}_0$ Imposed nodal fluid pressure

$\mathbf{P}_f$ Global vector of nodal fluid pressures

$\mathbf{P}_f$	Global vector of nodal fluid pressures
r	Filter radius
$\mathbf{S}$	Element matrix containing stresses
S_{sf}	Fluid-structure interface
$\mathbf{u}$	General vector of nodal structural displacements
$\mathbf{u}_s$	Global vector of nodal structural displacements
$\mathbf{v}$	Adjoint variable for buckling sensitivity analysis
$V(\mathbf{x})$	Volume fraction of existing material
$\overline{V}$	Prescribed final volume fraction
$\mathbf{x}$	Set of design variables
x_j	Design variable for the element j
x_p	Perturbed design variable

Greek Letters

β	Flip-limits parameter
ρ_{min}	Lower bound density
ρ_e	Element density
$\rho(\mathbf{x})$	Set of design variables as densities
Ω_f	Fluid domain
Ω_s	Structural domain
Ω_v	Void domain
Ω_e	Finite element domain
Γ_d	Dirichlet boundary
Γ_n	Neumann boundary
Γ_p	Fluid boundary
Γ_w	Hard wall boundary
$\Phi(\mathbf{x})$	Level set function
μ	General adjoint variable
σ_s	Cauchy stress tensor
σ_e	Element stress vector
σ_x	Normal stress component from x direction
σ_y	Normal stress component from y direction
τ_{xy}	Shear stress component from xy plane
λ_i	i^{th} buckling load factor
$\overline{\lambda}$	Prescribed buckling load factor lower limit
φ_i	i^{th} buckling mode
ϵ_v	Volume relaxation parameter
ν	Poisson ratio
τ	Convergence criteria parameter

Initials

ASI	Acoustic-Structure Interaction
BESO	Bi-directional Evolutionary Structural Optimization
ESO	Evolutionary Structural Optimization

FEA   Finite Element Analysis
FEM   Finite Element Method
FSI   Fluid-Structure Interaction
ILP   Integer Linear Programming
LSM   Level-Set Method
SIMP Solid Isotropic Material with Penalization
TOBS Topology Optimization of Binary Structures
TO   Topology Optimization

Contents

1 INTRODUCTION

Topology optimization (TO) has been increasingly adopted as a structural design tool in several engineering areas - from microstructures to large-scale problems [9]. This can be explained due to the highly efficient designs when compared to shape and parametric optimization, allowing non-intuitive solutions to be generated from full initial domains. Besides that, increasing computational capabilities and emerging academic research in this topic have led to a wider use of topology optimization, improving its efficiency and expanding its fields of application.

Classical topology optimization approach focuses on stiffness maximization under a certain volume constraint, neglecting stability requirements during the optimization process. This formulation usually leads to optimized structures with slender members - which exhibit poor stability performance [10]. The post-processing stage evaluates the optimized components and may require substantial changes that compromises their optimality. An alternative methodology is to include the stability parameter as constraint inside the compliance minimization problem, obtaining optimum solutions that also satisfy the stability performance. The typical optimization process and the proposed formulation are illustrated in Figure 1, based on [1].
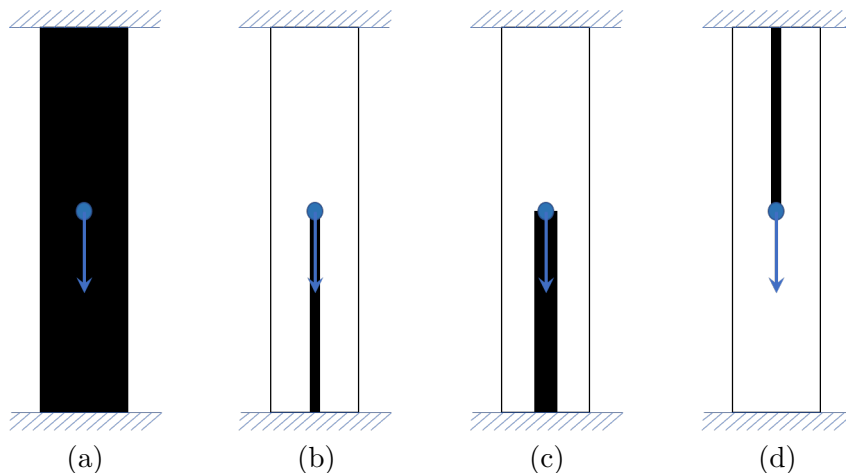
Figure 1: Representation of typical topology optimization stages: (a) initial domain; (b) optimum solution for maximum stiffness under a volume constraint; (c) solution after post-processing stage considering buckling analysis; (d) optimum solution considering buckling through the optimization problem [1].

Following classical approaches, the optimum solution shown in Figure 1 (b) ignores the buckling mechanism. After the post-processing phase, it is observed that solution (b) fits a critical case for buckling: thin member under a compression load. Therefore, a thicker cross-sectional area is designed so that a higher critical buckling load is achieved for the structure - see Figure 1 (c). However, the updated solution becomes less economical as more material is needed. An example of a more efficient solution can be seen in Figure 1 (d), where the buckling is considered inside the optimization problem as a constraint. To avoid this phenomenon, a tension member is designed using less material when compared to (c). Therefore, it is desirable to include as many relevant parameters as possible inside the optimization problem to obtain optimum solutions close to its final design, considering computational cost and prioritizing its efficiency.

Buckling can be defined as a failure mode due to a loss of stability caused by compressive loads, typically related to slender elements [11, 12]. When applied to TO problems, buckling is still a challenging topic and presents significant issues even when analyzed by a linear formulation [13]. Although buckling is inherently a geometrically nonlinear phenomenon, most researchers adopt linear buckling analysis for a smoother implementation and cheaper computational cost. This simplified approach, however, is still complicated, and explains the notable gap between compliance-only based optimization problems and those considering stability parameters [14–16].

Among the issues observed in buckling optimization problems, the following are commonly discussed [17, 18]:

- high computational cost due to repeated solution of large eigenvalue problems;

- high sensitivity of the results to the set of buckling modes considered in the formulation;

- activation and clustering of many buckling modes as the optimization progresses;

- existence of many local minima;

- artificial buckling modes.

TO problems in literature have applied buckling constraints for different structural models: e.g., beams [19], plates [20] and trusses [21]. Continuum domains, however, demonstrated a more complex approach explained both for its non-intuitive buckling behavior and several issues might emerge during the optimization process. For instance, the high computational cost corresponding to the buckling analysis, and the buckling sensitivity, may create an intractable optimization scenario, especially for large-scale cases [22]. Some numerical difficulties are intrinsically associated with the nature of the eigenvalue problem, such as mode switching and multiple eigenvalues. This problem takes place when distinct buckling modes correspond to repeated or closely-spaced buckling load factors - compromising the sensitivity analysis and the overall optimization convergence and demands efficient methods to solve them [23].

For 2D continuum structures problems, the Solid Isotropic Material with Penalization (SIMP) method stands out for buckling-constrained TO problems, followed by alternative approaches as the Bi-directional Evolutionary Structural Optimization (BESO) and the level-set method (LSM) [24]. The SIMP method has proven to be an effective and robust approach for various topology optimization problems. However, when dealing with buckling-constrained problems, this continuous relaxation method might present undesirable numerical issues related to the intermediate design variables, such as pseudo-buckling modes from low-density regions [25]. In order to solve such adversities, past works have focused on creating alternative methods to turn this approach feasible, such as homogenization methods, alternative material interpolations and penalty techniques [26–28].

Another challenge addressed in TO problems is the modeling of more complex conditions. Different environments require specific types of loads and each one acts in a specific way - e.g. acoustic, hydrodynamic, seismic, etc. When it comes to compression loads and buckling analysis, one might cite submerged structures, in which hydrostatic pressure loading is the prevalent condition applied to underwater components. This is the case of offshore engineering

structures, such as manifolds and wellheads. Figure 2 demonstrates a general case of hydrostatic pressure loading problem:
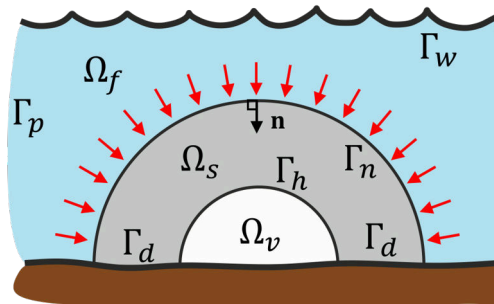
Figure 2: Structure subject to hydrostatic pressure loading: a case of a design-dependent problem. Where Ω_f is the fluid domain (such as water), Ω_s is the structural domain and Ω_v is the void domain. The boundary conditions are represented by: Γ_d - Dirichlet, Γ_n - Neumann, Γ_p - fluid and Γ_w - hard wall [2].

Such case imposes a careful implementation process because its behavior belongs to the design-dependent group of loads. The structure's boundaries generated at each optimization step define a new loading condition, requiring a nontrivial modeling when compared to fixed loads. Furthermore, hydrostatic pressure loadings typically act in compression over the structure elements - resulting in a potential condition for the buckling mechanism. Thus, it is important to investigate the effects of buckling for submerged structures when developing topology optimization methodologies [29].

In order to mitigate and solve some of those issues, different optimization methods have been studied and developed. Binary methods have shown interesting results when applied to buckling optimization problems and also to pressure loading cases [29]. One of the advantages of those methods when compared to classical ones - such as SIMP - is the absence of intermediate densities, which facilitates the modelling of surface loads. Even though a penalization is applied to avoid this scenario, elements that belong neither to the solid {1} nor the void {0} conditions impose numerical difficulties when modelling surface and buckling loads.

In this context, the Topology Optimization of Binary Structures (TOBS) arises as a promising approach to deal with buckling constraint TO problems coupled with pressure loads. Developed by Sivapuram and Picelli (2018) [30], this method adopts binary design variables and handles multiple constraints solved by a sequential integer linear programming scheme [31–33]. It holds the benefit of dealing with {0,1} variables and demonstrates a high potential when applied to buckling problems, a convenient approach among the available methods. Furthermore, the use of binary variables explicitly defines the structural boundaries where surface pressure loading can act. In comparison with BESO, the formal mathematical programming scheme by TOBS allows multiple constraints to be addressed without requiring new heuristics to be developed. This method is used in this study to solve the buckling-based problems for different boundary conditions. To the best of the authors' knowledge, this is the first work to consider buckling constraints in pressure loaded structural design via TO.

This work investigates the design of optimized structures in the presence of pressure loads with buckling constraints. The complexity of coupling those effects explains why previous authors have studied these phenomena either individually or associated with other scenarios, but none coupled into a general TO setting. Herein, a key tool to solve this unsolved problem

is to adopt the TOBS method considering both pressure loads and buckling constraints.

1.1 Objectives and contributions

Based on the discussed scenario, the **aim** of this work is to solve topology optimization problems considering buckling inside a design-dependent pressure load case. The TOBS method will be adopted because of the potential conveniences of binary variables when applied to the referred problem.

The **objectives** are:

1. to implement the FE-based structural analysis considering linear buckling and fluid pressure loads modelling.

2. to verify the linear buckling analysis via the Euler's critical load equation and its application on a topology optimization benchmark problem, e.g. the column under compression.

3. to solve buckling-constrained topology optimization problems of submerged structures.

4. to investigate and discuss the binary nature of the TOBS method when employed on buckling topology optimization problems.

1.2 Layout of the thesis

This thesis is structured as follows. Chapter 2 presents a comprehensive literature review of structural topology optimization, including the main works that bring relevant discussions considering buckling and design-dependent TO problems. Chapter 3 contains the fundamental concepts and theory regarding this research area: essential definitions and the standard formulation, available TO methods, sensitivity analysis, as well as a brief mathematical approach on linear buckling analysis and design-dependent loading. The applied methodology is discussed in Chapter 4, where the main algorithm to solve the proposed TO problem formulation is described and built up by a brief discussion for each step. Chapter 5 brings a few applications of the presented methodology through numerical examples, introduced by a verification of the linear buckling analysis implementation. The buckling constraint is initially investigated through a design-independent case, and later applied to pressure loading examples, discussing the obtained results. Finally, note-worthy points and the key contributions of this work are summarized in Chapter 6.

2 LITERATURE REVIEW

2.1 Topology optimization

First works related to structural optimization can easily be traced back to the 1700s, when Euler and Lagrange studied one-dimensional problem optimization, such as design columns and optimal cross-sectional areas for bar elements. Euler even focused on finding the best shape for gear teeth [34]. Since then, continuous research into the fields of mechanical engineering and advanced materials provided the principles theory for structural optimization problems, such as the work on variational calculus of Hamilton, and the optimum shape investigations of Clausen (1851) and Levy (1873) [35]. More advanced studies were particularly influenced by the emergence of computer science, allowing the calculation of complex mathematical algorithms and, thus, large-scale optimization problems [36]. Unlike size and shape optimization, whose aim is to find the optimum values for particular parameters, e.g. thickness and geometric shape, topology optimization focus on determining the connectivity, shape and void locations. Its greater design freedom represented a wide application in early conceptual and preliminary design phases of both academical and practical structural projects [37].

There are two main types of topology optimization research depending on the structure type: discrete and continuum. The first defines a case where the available material composes a low fraction of the design domain, resulting in thin elements and truss-like configurations [38]. Such problems usually seek to find the optimum number, positions and connectivity of the structural members, and many works have been developing research on this area, worth mentioning Prager and Rozvany (1977) [39].

In topology optimization of continuum structures, which is the focus of this work, higher volume fractions are distributed within a given 2D or 3D design domain, considering simultaneously the optimization of both external and internal shapes, as well as the number of inner holes [36]. Since the pioneer work of Bendsoe and Kikuchi (1988) [40], FE-based topology optimization of continuum structures have been investigated and applied to several structural response combinations, including heat transfer, fluid flow, acoustics, aeroelasticity and other multiphysics [37]. The representation of the topology usually occurs by values of material (usually called pseudo-densities) in an element of a finite-element mesh, e.g. SIMP, BESO and TOBS, or through an implicit functional that describes the solid/void region based on the boundary limits, as seen in Level-Set method [34].

Density-based methods are the most widely used methodology for the structural optimization and includes the popular Solid Isotropic Material with Penalization. It circumvents the challenging integer programming problem inherent to structural optimization problems by considering continuous variables and applying penalty methods to force a solid/void solution. Based on a generalized formulation, a variety of problems can be solved by the SIMP approach including mechanical stresses, natural frequency, displacement constraints, harmonic problems, fluid flow and non-linear systems [37]. Although very efficient in most of physical problems, the density variables imposes some difficulties as singularity in finite element matrices and spurious buckling modes. Regarding numerical issues related to stress, few works discussed some techniques to address the local nature of stress contents and the influence of block aggregations

as a solution [38, 41, 42]. Heat transfer and thermoelasticity have also been studied by Gersborg-Hansen et al. (2006) [43], Zhou and Li (2008) [44] and Wang et al. (2011) [45] using the SIMP method applied to FE-based topology optimization problems.

In contrast to density-based methods, discrete designs (in this work also called binary) deal with only solid/void variables and therefore are absent of the binary constraint relaxation in the problem setting [37]. Hard-kill methods were introduced by the Evolutionary Structural Optimization (ESO), proposed by Xie and Steve (1993, 1997) [46, 47], and later improved as a bi-directional ESO, where both removing and adding of elements were performed [48]. ESO/BESO methods generate solutions with crisply defined structural boundaries based on explicitly defined elements and, thus, free from gray material. Their application includes classical formulation as compliance minimization under volume constraint, but also multiphysics problems [49, 50], where clear definition of the structural boundary is critical for a good convergence process. Even bio-mechanical research area has been benefited from this class of methods, where the the study on tissue scaffolds using a wall shear stress criterion was developed by Chen et al. [51]. Recently, the Topology Optimization of Binary Structures method extended the class of binary TO methods by using sequential integer linear programming and has been effectively applied to different optimization problems - from microstructures settings [52] to turbulent fluid flow FSI conditions [53].

Composing the most recent development in the structural optimization scenario, boundary variation methods are based on an implicit representation of the structural boundary as a contour line, instead of explicit parametrization as seen in density-based (continuous and discrete) methods [37]. The level set approach, a well-known example of such methodology, was first used in topology optimization by Sethian and Wiegmann (2000) [54], introducing the analysis of a free boundary of a structure in the context of linear elasticity. Considering the modern formulation of the level set method, Wang et al. (2003) [55] discussed the velocity of points on the structural boundary applied to a stiffness maximization problem under volume constraint. Similarly to discrete methods, clear and smooth edges are obtained as a solution, naturally avoiding numerical issues related to intermediate densities and little post-processing is required [37]. Extent applications of this method have been studied for diverse physical settings, such as stress-based [56, 57], thermoelasticity [58, 59], fluid-flow [60, 61] and reliability-based problems [62, 63]. In general, many TO tools are available and based on robust formulations; but certain particularities should be taken into account on the engineer choice in order to perform the most suitable optimization process.

2.2 Buckling and optimization

Stability parameters have been studied since early times of structural optimization due to its importance for optimum designs effectiveness. Besides, classical optimization problems, e.g. compliance minimization under material constraint, usually generate stiff solutions that present poor stability [17]. The early works on this topic focused on studying mostly elementary structural components, such as beam and column models - where even a closed form expression was assigned as an optimality condition [64]. Plate models were then investigated for buckling optimization problems, defined by a much more challenging setting; promising discussions were

held on stability improvement solutions, such as reinforcement [65] instead of dealing with the thickness variation only [66]. Further research was deepened to the design of trusses, considering both local and global buckling modes. The first case constrained maximum stresses and displacements of individual members [67] while overall stability formulation was investigated by several authors, e.g. Khot et al. (1976) [68].

On the other hand, when it comes to buckling topology optimization problems for continuum models, significantly less research has been developed, which is explained both for an increase in complexity by a non-intuitive buckling development and the issues concerning the available density-based methods [17]. Numerical instabilities might occur when solving eigenvalue problems related to low density elements, as found in SIMP method [69]. This concern was initially discussed by Neves et al. (1995) [70], where a reinforcement technique was applied to a portal frame structure, modeled using FE-based continuous density elements. The effect of pseudo buckling modes related to low-density regions were circumvented by ignoring the geometrical stiffness matrices of elements with densities smaller than a prescribed value. This procedure was criticized by Bendsoe and Sigmund (2003) [38], affirming that discontinuity issues could arise in both objective functions and constraints. Thus, they suggested implementing a different penalization scheme for both stiffness matrix and geometric stiffness matrix, which has been applied in further works as studied by Lindgaard et al. (2013) [71].

In this context, a relevant progress regarding density-based methods has been observed recently, as seen in the works by Ferrari et al. (2021) [14–16], which solved buckling constrained problems with a 250-line implementation code in MATLAB - see Figure 3 (c). The column under compression is a benchmark TO problem that employs buckling constraint and has been investigated by a few authors. Figure 3 shows the solutions from Browne et al. (2013), Gao and Ma (2015) and Ferrari et al. (2021) [16, 18, 26].
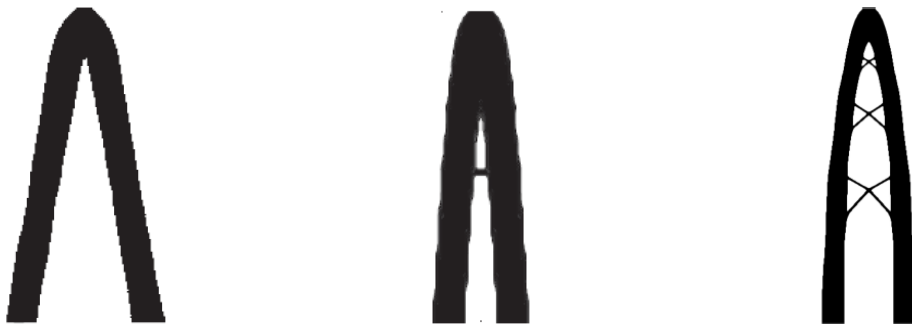
(a) Browne et al. (2013) [26]   (b) Gao and Ma (2015) [18]   (c) Ferrari et al. (2021) [16]

Figure 3: Different solutions for the column under compression problem applied to a buckling-constrained TO formulation.

As previous stated, discrete methods - such as BESO, and recently TOBS - are able to solve TO problems by eliminating intermediate densities and obtaining final solutions of structure or simply void elements. A potential advantage of this fact is that such solvers are not prone to numerical instabilities related to grayscale regions when solving eigenvalue problems [37]. Recent results have shown effective applications of binary variables in buckling constrained TO problems, e.g. ESO in Rong et al. (2001) [72]. In order to extend the potential of discrete

methods in such formulation, the purpose of this work is to investigate the TOBS method as an unexplored and promising application for TO problems considering stability parameters and discuss its particularities for submerged structures.

2.3   Design-dependent pressure loads

Design-dependent loads have been considered for purely structural design, such as in self-weight problems [50,73], thermoelastic design [58,74] and pressure loads [75,76]. Surface loading, e.g., pressure, is the focus for the proposed project since a major part of the offshore structures are pressure loaded due to the interaction with hydrostatics, acoustics, wind loads or water flow.

The first work to consider a fluid phase as means to model pressure loads into topology optimization was by Sigmund and Clausen [3]. The authors used the SIMP method, in which a continuous variation of material densities within the bounds [0,1] is used as parameterization, 1 for completely solid material and 0 for void. Regions where density is between 0 and 1 represents unrealistic material and the intermediate material densities can make the structural boundary fuzzy and ill-defined, as indicated in Fig. 4.
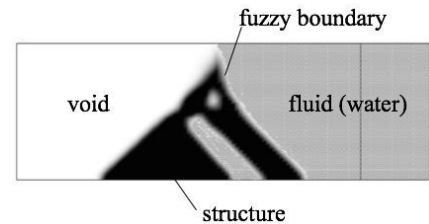
Figure 4: Dam design from Sigmund and Clausen (2007) [3].

The challenge becomes to extract the correct surface within the fuzzy boundary where the pressure load should be accurately imposed, especially during early stages of optimization where a large amount of intermediate densities are present. The solution proposed by Sigmund and Clausen [3] was to use the mixed finite element formulation, where structural displacements and fluid pressures are considered as primary variables, both interpolated in a single element. Figure 4 shows the design of a dam subject to only hydrostatic water pressure [3]. Another example (piston head model) that applied the SIMP method is presented in Fig. 5.

Figure 5: SIMP by Sigmund and Clausen (2007) [3].

The interface between the solid and fluid fields is not clearly defined during optimization, but the use of a mixed displacement-pressure finite element circumvented the surface extraction step. The same idea was extended to acoustic-structure interaction (ASI) [77] and fluid-structure interaction (FSI) [78] problems. However, the use of mixed finite element methods leads to some drawbacks, such as numerical pathologies (violation of the inf-sup conditions [79]) and the existence of fluid and structure overlapping domains, which increases the computational costs and reduces the efficiency of the method, as reported by Yoon [78]. Therefore, a few authors explored the use of other optimization methods, which rely on explicitly defined 0-1 designs and separate governing equations, namely the Level Set Method [80] and the Bi-directional Evolutionary Structural Optimization [81].

The BESO is a gradient-based method and uses discrete only {0, 1} design variables, without intermediate densities. Consequently, the structural boundaries are always explicitly defined and the modeling of different physics is straightforward. Picelli and co-authors developed a BESO method for design-dependent pressure loading problems [82], acoustic-structure interaction

design [83, 84] and, recently, fluid-structure interaction problems [85]. The BESO method, however, lacks of a mathematical optimizer and the inclusion of different types of constraints, such as buckling, rather than volumetric ones, might not be straightforward [30].

Seeking to study more complex conditions and provide structural designs whose applications are well modeled, this project aims to combine two different optimization problem parameters: pressure loading and buckling constraints. Adding to this setting as the proposed optimization solver, the TOBS method shares the advantages of using $\{0, 1\}$ variables. Therefore, the methodologies developed by Picelli and co-authors [83, 84] are the basis when it comes to design-dependent pressure loads (Fig. 6).

Figure 6: TOBS by Sivapuram and Picelli (2020) [4].

Furthermore, the TOBS generalizes the optimization problem by using sequential linearization, which allows multiple constraints to be included directly. Hence, the TOBS is a fair candidate to address buckling constraints of submerged structures for the first time.

3 THEORETICAL FRAMEWORK

3.1 Structural optimization

In a short definition, optimization is related to any operation that seeks the best outcome while satisfying given restrictions. Humankind has always been influenced by their natural surroundings and has tried to save energy and resources in order to maximize output or profit. A clear example of this philosophy is the invention of the lever or the pulley mechanisms as a tool to increase the mechanical efficiency of heavy tasks. In that context, the best design possible that a structure might have has been defined as an "optimum design", and was the main research topic that commenced the structural optimization development [6].

When it comes to the structural project, two main approaches might be adopted: the analysis or the optimization ones. The first consists of analysing different possible configurations of a structure. Each design is then evaluated for specific parameters performance, and their results are used to select the best option. The analysis approach efficiency depends on the number of parameters adopted, seen that the number of analysis grows exponentially as the possibility of different designs increases. Therefore, this method turns out to be unfeasible for complex structural problems and/or to evaluate a large number of possible solutions [86].

On the other hand, the optimization - or synthesis - approach is composed by computational methods that rationally look for the optimum configuration for the given project. That is, the algorithm will seek, among the possible solutions space, the combination that provides the best project performance. Therefore, the optimization definition is properly used when related to mathematical methods that systematically search for the optimum the design. This term is misused when applied to methods that consider a significant amount of design options and pick the best one based on trial and error [86].

3.1.1 Brief history of optimization

The rising of optimization methods is dated to the time of Newton, Lagrange and Cauchy. The contributions of those mathematicians made feasible the existence of modern optimization methods. The differential calculus methods applied to optimization was possible because of Newton and Leibnitz findings to calculus. The addition of constraints inside the optimization occurred after Lagrange's studies on unknown multipliers. Cauchy was responsible to apply for the first time the steepest descent method to solve unconstrained minimization problems [87].

Despite the absence of computational resources, Maxwell and Mitchell were important researchers that applied optimization concepts in obtaining optimum designs between the 19th and the 20th centuries. First, Maxwell, in 1872, studied a bridge-structure optimization, using the available Theory of Elasticity concepts and he calculated its stress field and its directions. According to Maxwell, the optimum design would be a set of unidimensional structures arranged following the stress field lines.

Later in 1904, Michell used some of Maxwell theories and applied to different study cases seeking the optimum solution for the minimum material possible. Michell was able to confirm some of Maxwell results and deepen his research considering several optimization problems. Figure 7 presents some of Michell's optimized structures taken from his original work entitled:

"The limits of economy of material in frame-structures", published in 1904 [5].
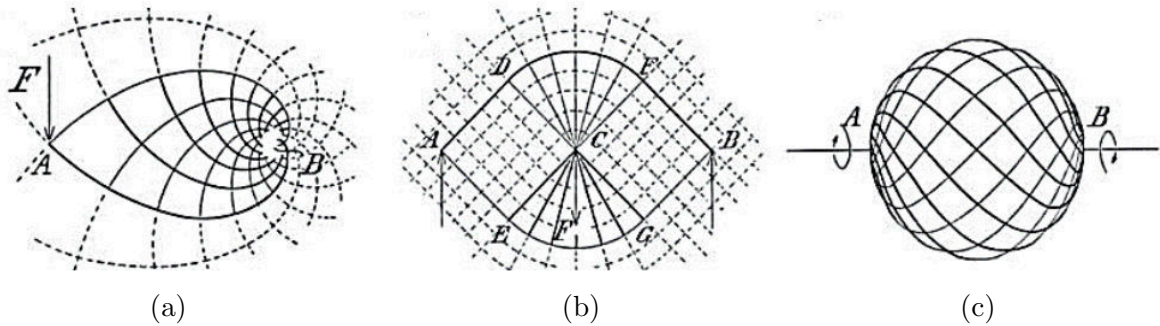
Figure 7: Three applications of Michell optimization work: (a) cantilever, (b) simply supported beam and (c) torsion bar [5].

As observed in Fig. 7, the structures' lines compose a pattern that became notorious and widely known as Michell's pattern. Decades further, once computational tools were available, researchers were able to assure this pattern's optimality and find it in several optimized problems as the best solution [88].

After Michells work, no significant study had been developed until the availability of computational tools, driven mainly by the aerospace industry. During the 50 and 60s, this engineering field were focused on creating minimum weight design of structures due to the high impact that excess material has on aircrafts' efficiency. From the rising of the Finite Element Method (FEM) and other structural analysis software, the study on structural optimization methods returned to be developed and discussed [6]. Nowadays, sustainability, material use efficiency and technological competition are some of the factors that boost the optimization area and improves its methods and feasibility applications.

3.2   Fundamentals of structural optimization

Understanding the structural optimization problem requires the knowledge deepening in essential concepts and basic fundamentals regarding this broad topic. At first, three main elements of problem formulation will be shortly explained: design variables, objective function and constraints.

3.2.1   Elements of optimization problem

- Design variables

The idea of structural optimization is to improve the structure's performance based on the possibility to change some parameters. These modifications are related to the defined variables that are free to assume different values inside the project. Such parameters are called *design variables* and are usually designated by a vector $\mathbf{x} = (x_1, x_2, ..., x_n)$. Some examples of design variables are cross-sectional dimensions, member sizes, densities, among others.

Design variables can assume *continuous* or *discrete* values. The first class can take any value considering a range of variation. Examples of usual continuous variables in optimization problems are moment of inertia of a beam and its cross-sectional dimensions. Discrete design variables, however, must consider only predefined available values - such as binary variables [6].

- Objective function

A reference to measure the optimization problem's efficiency is defined by a determined function - $f(\mathbf{x})$ - or multiple ones - $\mathbf{f}(\mathbf{x}) = [f_1(\mathbf{x}), f_2(\mathbf{x}), ..., f_p(\mathbf{x})]$. Such element is designated as *objective function*. Many structural parameters can be considered as an objective function, such as stiffness, volume, stresses, buckling loads and vibration frequencies. The coupling of two or more objective parameters can also be implemented and defines a *Multicriteria Optimization* problem.

Haftka and Gürdal (1992) [6] expresses that the adoption of *multiobjective function* should be avoided due to high complexity involved in solving such problems. Some techniques are used to turn multiple objectives into one, e.g. generating a composite objective function that replaces all the objectives or select the most important function and impose limits to the others.

- Constraints

Most of optimization problems are subject to restrictions due to several reasons: material availability, cost, physical performance, and others. These established restrictions involving the design variables are referred as *constraints*. When these bounds define upper and lower values for the variables, they are denominated as *inequality constraints* - generally expressed as $g(\mathbf{x})$. On the other hand, if a specif value must be achieved by the design variable, an *equality constraint*, denoted as $h(\mathbf{x})$, is applied. This last approach is not desirable - specially for nonlinear optimization problems that are unable to handle equality constraints [6].

3.2.2 Standard formulation

The usual optimization problem including the previous concepts is formulated as:

$$
\begin{aligned}
\underset{\mathbf{x}}{\text{Minimize}} \quad & f(\mathbf{x}) \\
\text{Subject to} \quad & g_i(\mathbf{x}) \leq 0, \quad i \in [1, N_g] \\
& h_b(\mathbf{x}) = 0, \quad b \in [1, N_e]
\end{aligned}
\tag{1}
$$

where $\mathbf{x}$ represents the vector of design variables, $g_i(\mathbf{x})$ and $h_b(\mathbf{x})$ denote the inequality constraints and the equality constraints, respectively. The definition of *minimization* problem does not mean that a *maximization* approach is restricted. As a matter of fact, any maximization can be explored by minimizing its negative [6].

3.2.3 Types of structural optimization

The optimization problem can be classified into three main types: parametric, shape and topology optimization. They address different aspects on the optimization purpose and freedom to change the design. Figure 8 illustrates a similar example solved for the three optimization types.

- Parametric optimization: it is defined when the domain of the design model and state variables are previously known and fixed throughout the optimization. Its goal is to find

(a) Parametric optimization   (b) Shape optimization   (b) Topology optimization
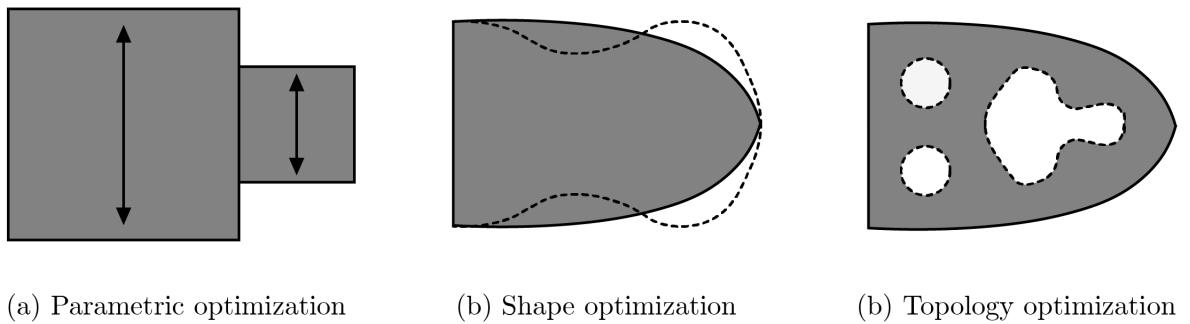
Figure 8: The main approaches for structural optimization: parametric, shape and topology methods.

the optimum parameter of a given structure, e.g. thickness distribution of a plate, cross-sectional area of a beam, among others. The potential change on the desired parameter allows the optimization solver to find an optimum performance for a physical quantity, such as deflection [6]. Figure 8(a) shows an example where a beam is optimized regarding its bars' thickness.

- Shape optimization: the structure's shape is defined as the design variable of the optimization. The domain's boundaries - position and geometry - are modified in order to improve the objective function. This optimization type allows a more significant change when compared to parametric approach, and therefore defines a more complex formulation. An application of this optimization can be seen in Figure 8(b): after the optimization process, the boundaries had its shape changed.

- Topology optimization: Bendsoe and Sigmund (2003) defines this class as the one with a higher potential of change and is based on seeking the best material distribution within a specified region. The advantage of topology optimization is that the solver is free to obtain the optimum layout, and not only the size or shape of the structure. Features as the number, location and shape of holes, as well as the connectivity of the domain is also the focus of TO. The complexity of this approach explained the reasons why topology optimization is the youngest among the available methods and emerged along the computational power. Figure 8(c) displays an example where a full domain structure is optimized and exhibits the best material distribution, holes and connections for the given formulation.

3.3 Topology optimization

The objective of applying topology structural optimization is to determine the best distribution of a given material. In other words, we aim to obtain which points are solid 1 and which points should remain void 0. This common approach seeks to find the final design variable vector containing {0,1} values, given as

$$x_j(\mathbf{x}) = \begin{cases} 1 & \text{for } \Omega_s \\ 0 & \text{for } \Omega_v \end{cases} \qquad (2)$$

where x_j indicates whether the element j belongs to the solid domain Ω_s or the void domain Ω_v [6]. The Finite Element Method is commonly used to support the optimization procedure by discretizing the full domain into finite elements. The representation of the material distribution is done by assuming solid elements as black and void elements as white. This process is illustrated in Figure 9, where an optimum design is obtained by a topology optimization:
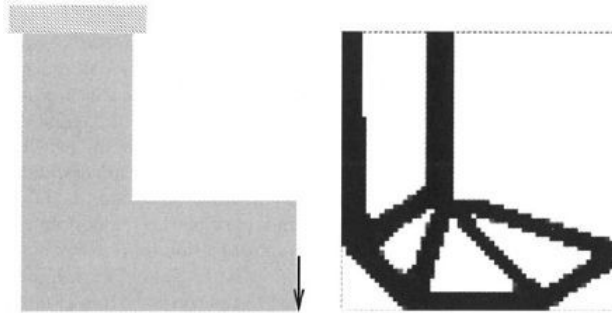
Figure 9: Example of an optimized design for a given structural problem [6].

Fig. 9 shows the initial domain (left) that has been discretized into 60x60 elements, and the minimum compliance design (right), obtained for a final volume of 47%. It is expected that the final design presents only void or solid elements - that is, discrete variables {0,1}.

Nonetheless, dealing with only integer variables is a more challenging approach. In that context, a few alternative methods have been proposed to solve the TO problem prioritizing a feasible computational cost and assured efficiency. The most notorious methods are:

- Density-based methods

These methods define the most used alternative to prevent numerical issues with purely [0-1] variables. Density-based TO methods express the material distribution as pseudo-densities $\rho(\mathbf{x})$ which vary from a ρ_{min} - to avoid singularity problems - to 1, representing the solid state [38]. Since FEM is usually adopted, each element density is assigned as ρ_e. The intermediate densities are undesirable and a penalization is introduced to force them to achieve a {0,1} pattern. A common density-based formulation, based on Finite Element Analysis (FEA), is expressed as [7]:

$$
\begin{aligned}
&\underset{\rho(\mathbf{x})}{\text{Minimize}} && f(\rho(\mathbf{x}), \mathbf{u}) \\
&\text{Subject to} && \mathbf{K}(\rho(\mathbf{x}))\mathbf{u} = \mathbf{F}(\rho(\mathbf{x})) \\
& && g_i(\rho(\mathbf{x}), \mathbf{u}) \leq 0, \quad i \in [1, N_g] \\
& && h_b(\rho(\mathbf{x}), \mathbf{u}) = 0, \quad b \in [1, N_e] \\
& && \rho_{min} \leq \rho(\mathbf{x}) \leq 1
\end{aligned}
\tag{3}
$$

where $f(\rho(\mathbf{x}), \mathbf{u})$ is the objective function, and $\mathbf{Ku} = \mathbf{F}$ is the static equilibrium equation that depends on the stiffness matrix $\mathbf{K}(\rho(\mathbf{x}))$, the displacement vector $\mathbf{u}$ and the force vector $\mathbf{F}(\rho(\mathbf{x}))$.

The most notorious example of this class of methods is the Solid Isotropic Material with Penalization [38], which defines a density-based material model and is widely applied in TO problems for its robust and relatively simple implementation. The SIMP model defines the proportional stiffness of each element j as

$$E(x_j) = \rho(x_j)^p E_0, \tag{4}$$

which is based on its penalized density $\rho(x_j)^p$, where p is the penalty value, and the material property is represented by E_0.

- Discrete methods:

In order to avoid the issues related to the grayscale intermediate densities, discrete methods have been developed to obtain [0-1] final designs and crisply defined structural boundaries. Discrete methods generally work with binary variables, where $x_j = 1$ defines a solid finite element and $x_j = 0$ when it is void [89]. A few features demonstrate similarity between discrete and density-based methods, such as resembling optimization procedures and dealing with gradient information. The Bi-directional Evolutionary Structural Optimization [81] and the Topology Optimization of Binary Structures [30] are established examples that develop this approach. Their formulation, instead of working with density ρ as design variables, utilizes only 1 or 0 values.

- Boundary variation methods:

Another usual method changes the optimization perspective by considering the structure's boundaries as design variables instead of the elements' densities. This class assumes a level set function Φ, describing the material domain as [7]

$$x_j(\mathbf{x}) = \begin{cases} \Phi(\mathbf{x}) > c & \text{for } \mathbf{x} \in \text{material domain,} \\ \Phi(\mathbf{x}) = c & \text{for } \mathbf{x} \in \text{interface,} \\ \Phi(\mathbf{x}) < c & \text{for } \mathbf{x} \in \text{void,} \end{cases} \tag{5}$$

where c is usually defined as 0. The Heaviside function is a common approach to define the structure's geometry and its optimum layout. It is also a component of the Level-set Method (LSM), a robust and well-known example of a boundary variation approach.

3.3.1 The TOBS Method

The Topology Optimization of Binary Structures has been used in this work to develop the proposed investigations. Developed by Sivapuram and Picelli [30], this methodology combines four well known numerical ingredients: sequential approximate optimization problems, binary design variables, sensitivity filtering and integer linear programming (ILP). Its generic formulation as a binary approach with inequality constraints is stated as

$$\begin{aligned} \underset{\mathbf{x}}{\text{Minimize}} \quad & f(\mathbf{x}), \\ \text{Subject to} \quad & g_i(\mathbf{x}) \leq \overline{g}_i, \ i \in [1, N_g], \\ & x_j \in \{0, 1\}, \ j \in [1, N_d], \end{aligned} \tag{6}$$

where f is the objective function, which depends on the design variables vector $\mathbf{x}$ of size N_d. The inequality constraints are defined by g_i, its upper limit is $\overline{g}_i$ and the number of inequalities are expressed by N_g.

As most of topology optimization problems are highly nonlinear and nonconvex, the TOBS method uses the Taylor's series approximation theory by generating linear suboptimization problems sequentially which is solved by integer linear programming methods [8]. Thus, the general TO problem - Eq. 6 - can be rewritten as

$$
\begin{aligned}
f(x) &= f(x^k) + \frac{\partial f(x^k)}{\partial x} \cdot \Delta x^k + O(||\Delta x^k||_2^2), \\
g_i(x) &= g_i(x^k) + \frac{\partial g_i(x^k)}{\partial x} \cdot \Delta x^k + O(||\Delta x^k||_2^2),
\end{aligned}
\tag{7}
$$

where k is the iteration number, $O(||\Delta x^k||_2^2)$ is the truncation error and the design variable changes are denoted by Δx^k. The changes on the design variables are defined so that the design variables keep their binary nature. Thus, if the element is solid $x_j = \{1\}$, the change should be either $\{0\}$ to remain solid or $\{-1\}$ to become a void. The opposite definition occurs for void elements, which changes might be either $\{0\}$ to remain void, or $\{+1\}$ to become a solid element. These bounds can be stated as

$$
\begin{cases}
0 \leq \Delta \mathbf{x}^k \leq 1, & \text{if } x_j^k = 0, \\
-1 \leq \Delta \mathbf{x}^k \leq 0, & \text{if } x_j^k = 1.
\end{cases}
\tag{8}
$$

A constraint is introduced to ensure the truncation error $O(||\Delta \mathbf{x}^k||_2^2)$ to be small, maintaining the linearization valid via a variable β. This variable limits the amount of changes of design variables from void to solid and vice-versa at each iteration, controlling the truncation error. This constraint is expressed as

$$
||\Delta \mathbf{x}^k||_1 \leq \beta N_d,
\tag{9}
$$

where β limits the amount of changes based on the total amount of design variables (N_d). Based on the linearized functions (Eq. 7), the general optimization problem is solved as an approximate integer subproblem given by [8]

$$
\begin{aligned}
&\underset{\Delta x^k}{\text{Minimize}} \; \frac{\partial f(x^k)}{\partial x} \cdot \Delta x^k, \\
&\text{Subject to } \frac{\partial g_i(x^k)}{\partial x} \cdot \Delta x^k \leq \overline{g}_i - g_i(x^k) := \Delta g_i^k, \; i \in [1, N_g], \\
&\qquad\qquad ||\Delta x^k||_1 \leq \beta N_d, \\
&\qquad\qquad \Delta x_j^k \in \{-x_j^k, 1 - x_j^k\}, \; j \in [1, N_d].
\end{aligned}
\tag{10}
$$

Integer Linear Programming (ILP) can be used to solve the linearized optimization problem Eq. (10). This approach is similar to Linear Programming (LP), except for the additional constraints to obtain only integer solutions. In this work, the branch-and-bound algorithm from

the CPLEX library - developed by IBM - is used to solve the ILP problem. In this approach, the problem is initially solved by LP without any bounds, using a linear optimization technique, such as the Simplex method. Then, the initial solution is subjected to inequality constraints seeking to find the integer solution [90]. The computational cost required by the branch-and-bound algorithm by CPLEX is minor when compared to the FEA, as discussed by [32, 91].

Sivapuram and Picelli [30] also showed that the TOBS method can solve the minimization of structural volume subject to compliance considering a design-dependent pressure loading. Its capability to handle multiple nonvolume constraints [91, 92] allowed the addition of the buckling constraint for the proposed multiphysics optimization problem.

3.4   Sensitivity analysis: available methods

The term sensitivity characterizes the effect on an input change on the output. For structural topology problems, this designation describes the derivatives evaluation regarding the response functions with respect to the design variables. For a gradient-based topology optimization process, the most time consuming procedure is the sensitivity analysis [93]. This crucial step are composed by the derivatives calculation that provides to the solver the required information that leads to the proper optimization convergence. For this reason, few sensitivity methods have been developed and they might be grouped in three main categories: global finite differences, discrete derivatives and variational derivatives [94]. Keulen et al. (2005) also affirms that the decision on which method to apply depends strongly on the structure type, the computer program capability and accuracy. A brief explanation for each method is discussed as follows:

3.4.1   Global finite difference method

Considered the simplest technique for computing derivatives, the finite different method is often computationally expensive yet very popular and easy to implement. It is also applied to certify the efficiency of analytical approaches [95]. For this method, the Finite Element Analysis is fully performed considering a perturbation applied to each design variable and its accuracy depends on the step size adopted. The most popular techniques are the forward and backward differences, when compared to the central approach. This latter might present a higher accuracy, but also requires an addition FEA calculation and, therefore, a more expensive computational choice.

The errors involved in this method are related to the step size, i.e. value of the perturbation, since both too small or large values can jeopardize the derivatives calculation. Truncation errors occur when big values are assumed for the step size and inaccuracies might emerge associated to the Taylor series expansion. On the other hand, extremely small values cause insignificant changes in the design variables response, which are subject to round-off errors and ill-conditioning of the TO problem [93].

When applied to the static equilibrium equation, the finite difference method requires the solution of the linear system of equations $\mathbf{Ku} = \mathbf{F}$, where u is the displacement vector of the original design variables x. The perturbed design variable is $x_p = x + \Delta x$, where Δx is the step size. The sensitivities for the displacement vector with respect to the design variable x through a forward difference method is [93]:

$$\frac{\partial \mathbf{u}}{\partial x} \approx \frac{\mathbf{u}(x + \Delta x) - \mathbf{u}(x)}{\Delta x} \tag{11}$$

where $\mathbf{u}(x + \Delta x)$ is obtained by solving $\mathbf{K}(x + \Delta x)\mathbf{u}(x + \Delta x) = \mathbf{F}(x + \Delta x)$. Although global finite difference approximation can be easily applied for response functions that are not solved by analytical approaches, this sensitivity method is very time consuming and are not practical for large discretized problems [96].

3.4.2 Variational derivatives

This sensitivity approach is applied to structures whose structural behavior is expressed by continuum equations, e.g. beams and shells [94]. Such derivatives are obtained by differentiation of the governing equations with respect to the design variables before they are discretized. In other words, this sensitivity technique can be described as a variation of a function, and is solved after the structure has been discretized [96]. This sensitivity analysis method is desirable for problems where the discretized equations are not available through the source code access, such as observed in many popular structural analysis programs [95].

3.4.3 Discrete derivatives

For this class of sensitivities, the derivatives are computed for the characteristic parameters, such as displacement, stresses, volume, buckling etc, which compose the objective and constraint functions. Unlike the variational sensitivity analysis, the discrete approach is based on the a differentiation of the discretized equations. Discrete derivatives can be computed in the direct and the adjoint formulation [96].

- Direct sensitivity analysis

Direct sensitivity approach adopts an explicit evaluation of the state derivative for each design variable. This method is useful when the stored state derivatives are used in many response functions. However, for FE-based To optimization problems this is rarely observed. For such cases, where the number of design variables are extremely large when compared to the the number of response functions are small, the direct sensitivity analysis is not applicable [96]. The derivative of the displacement vector u with respect to the design variable through the direct approach is

$$\frac{\partial \mathbf{u}}{\partial x} = \mathbf{K}^{-1} \left(\frac{\partial \mathbf{f}}{\partial x} - \frac{\partial \mathbf{K}}{\partial x} \mathbf{u} \right) \tag{12}$$

- Adjoint sensitivity analysis

As a much more efficient option to perform the sensitivity analysis for most FE-based TO problems, the adjoint method is extensively applied for cases with a large number of design variables and only a few response functions. This procedure can be illustrated for a derivative a function $f(\mathbf{x}, \mathbf{u})$ with respect to x. The chain rule applies once the function depends on $\mathbf{u}$ and implicitly on x

$$\frac{df}{dx} = \frac{\partial f}{\partial x} + \left(\frac{\partial f}{\partial \mathbf{u}}\right)^{\mathrm{T}} \frac{\partial \mathbf{u}}{\partial x} = \left(\frac{\partial f}{\partial \mathbf{u}}\right)^{\mathrm{T}} \frac{\partial \mathbf{u}}{\partial x} \tag{13}$$

where $\partial f/\partial x$ is zero in this example because the function does not depend explicitly on x. Adopting the definition of the derivative of $\mathbf{u}$ with respect to x in Eq. 12, Eq. 13 can be rewritten as

$$\frac{df}{dx} = \left(\frac{\partial f}{\partial \mathbf{u}}\right)^{\mathrm{T}} \mathbf{K}^{-1} \left(\frac{\partial \mathbf{F}}{\partial x} - \frac{\partial \mathbf{K}}{\partial x}\mathbf{u}\right). \tag{14}$$

Since $\mathbf{K}$ is a symmetric matrix, Eq. 14 is then expressed as

$$\frac{df}{dx} = \left(\mathbf{K}^{-1}\frac{\partial f}{\partial \mathbf{u}}\right)^{\mathrm{T}} \left(\frac{\partial \mathbf{F}}{\partial x} - \frac{\partial \mathbf{K}}{\partial x}\mathbf{u}\right). \tag{15}$$

An adjoint variable μ is inserted in Eq. 15 in order to allow the equation system to be solved for the displacement derivative of the objective. In other words, this procedure does not require a calculation for each $\left(\dfrac{\partial \mathbf{F}}{\partial x} - \dfrac{\partial \mathbf{K}}{\partial x}\mathbf{u}\right)$, also known as pseudo load vector. Instead, the system is solved only once and the sensitivity analysis can be obtained by a scalar product of the adjoint variable and the pseudo load vector.

$$\frac{df}{dx} = \mu^{\mathrm{T}} \left(\frac{\partial \mathbf{F}}{\partial x} - \frac{\partial \mathbf{K}}{\partial x}\mathbf{u}\right). \tag{16}$$

The adjoint formulations require little computational memory and, thus, less processing time when compared to direct approaches. Several structural responses can be derived using adjoint variables, and this work, specifically, applies this method to compute the buckling load factor sensitivities.

3.4.4 Semi-analytical method

This method combines the features of both discrete and finite difference approaches. The semi-analytical technique is particularly beneficial when the analytical formulation requires complicated implementation or even inaccessible sensitivity routines [96]. For instance, the sensitivity computation is comprehended as semi-analytical if the derivatives of the stiffness matrix with respect to the design varible x in Eq. 12 is obtained via a forward difference method as

$$\frac{\partial \mathbf{K}}{\partial x} \approx \frac{\mathbf{K}(x + \Delta x) - \mathbf{K}(x)}{\Delta x} \tag{17}$$

An elemental benefit of this class of sensitivity analysis is that minor implementation effort is required and the expected numerical cost. However, the drawbacks related to finite difference methods, e.g. errors, must be evaluated and analysed for each optimization problem.

3.5   Finite Element Analysis

3.5.1   Equilibrium equations

Initially, design domains will be divided into square two-dimensional 4 node elements, with 2 degrees of freedom per node. To save computational time, all elements share the same dimensions, so that the element stiffness matrix $\mathbf{K}^{(e)}$ can be calculated only once. As the 2D cases are successfully analyzed, three-dimensional problems will be implemented and developed, seeking a feasible computational cost.

To calculate the structure's displacements, it is applied the equilibrium equation for static problems, shown below:

$$\mathbf{Ku} = \mathbf{F} \tag{18}$$

where $\mathbf{K}$ is the global stiffness matrix, $\mathbf{u}$ is the displacement vector and $\mathbf{F}$ the force vector applied to the structure.

For the proposed problems, the static analysis is applied to flexible structures under incompressible pressurized fluids. Such fluid-structure coupling is modelled considering small displacements for a linear elastic solid domain and inviscid and irrotational fluid domain, as studied by Picelli et al. (2015) [82]. The proposed problem formulation is further discussed by Zienkiewicz and Bettess (1978) [97], Morand and Ohayon (1995) [98] and Axisa and Antunes (2007) [99].

Since the main problem is based on pressure loads, a hydrostatic fluid is introduced with one pressure degree of freedom per element. The system then requires a coupling of both fluid and structural domains. Their components act together in the normal direction of the boundary, and the equilibrium condition is given by Eq. 19:

$$\sigma_s \mathbf{n} = -\mathbf{P}_f \tag{19}$$

where $\mathbf{P}_f$ is the vector of the nodal fluid pressures, σ_s is the Cauchy stress tensor and $\mathbf{n}$ is the normal vector. The finite element method can be used as an approximation to model the force that acts on the structure deriving from the fluid pressure as

$$\mathbf{f}_{fs} = \int_{S_{sf}} \mathbf{N}_s^{\mathrm{T}} \mathbf{n} \mathbf{N}_f dS_{fs} \mathbf{P}_f, \tag{20}$$

where the structure and fluid finite element shape functions at the interface are represented by $\mathbf{N}_s$ and $\mathbf{N}_f$, respectively. The spatial coupling matrix L_{fs} is then defined as

$$\mathbf{L}_{fs} = \int_{S_{sf}} \mathbf{N}_s^{\mathrm{T}} \mathbf{n} \mathbf{N}_f dS_{fs}. \tag{21}$$

Considering Eq. 20 and 21, the coupling force can be rewritten in a discrete form:

$$\mathbf{f}_{fs} = \mathbf{L}_{fs} \mathbf{P}_f, \tag{22}$$

The equilibrium condition expressed in (19) leads to a one-way coupled problem discretized using the FEM - see Eq. (23). This equation describes the hydroelastic equilibrium problem.

No external loads are applied. The pressure loads are generated by imposing pressure values $\mathbf{P}_0$ as Dirichlet boundary conditions in $\mathbf{P}_f$.

$$\begin{bmatrix} \mathbf{K}_s & -\mathbf{L}_{fs} \\ 0 & \mathbf{K}_f \end{bmatrix} \left\{ \begin{array}{c} \mathbf{u}_s \\ \mathbf{P}_f \end{array} \right\} = \left\{ \begin{array}{c} 0 \\ 0 \end{array} \right\}, \tag{23}$$

where $\mathbf{K}_s$ and $\mathbf{K}_f$ are the stiffness matrices of the structural and the fluid domains, respectively. $\mathbf{L}_{fs}$ is the coupling matrix, calculated at the fluid-structure interface. It is worth pointing out that $\mathbf{L}_{fs}$ can be computed in a straightforward manner when using binary fluid-structure topologies, such as it is done in the BESO and the TOBS methods.

3.5.2 Linear buckling analysis

Conventional compliance minimization requires solving only one equilibrium condition: Eq. 18. The buckling constraint necessitates solving an additional eigenvalue problem. For a linear buckling analysis the stresses are also required. The stresses are evaluated at the Gauss integration points, defined for each element, and used to determine the stress stiffness matrix $\mathbf{K}_\sigma$. Once this global matrix is computed, the eigenproblem that governs the linear buckling analysis is described as follows:

$$(\mathbf{K}[\mathbf{x}] + \lambda \cdot \mathbf{K}_\sigma[\mathbf{x}, \mathbf{u}(\mathbf{x})])\varphi = 0. \tag{24}$$

The eigenpairs (λ, φ) consist of the critical load factors λ_i and the corresponding buckling modes φ_i. Structural design is usually made considering only the first few buckling modes, so a set M of lower buckling mode is computed. In this work, we computed the first 20 buckling modes and their corresponding load factors. Negative buckling load factors have no practical meaning, as such buckling modes are associated to the reference load pointing to the opposite direction and therefore, only positive buckling load factors are considered [100]. For the proposed problems, we obtained sufficient positive eigenvalues when computing the first 20 eigenpairs (λ, φ). The eigenvalues are sorted in ascending order with λ_1 being the smallest, and is called, the critical buckling load factor $(\lambda_{cr} = \lambda_1)$. The critical load (F_{cr}) for the structural system is then defined as:

$$F_{cr} = \lambda_1 \cdot F_0, \tag{25}$$

where F_0 is the original force vector applied on the structure.

In order to solve the eigenvalue problem Eq. 24, the stress stiffness matrix $\mathbf{K}_\sigma$ is obtained by the assembling $\mathbf{K}_\sigma^{(\mathbf{e})}$, which is computed using:

$$\mathbf{K}_\sigma^{(e)} = \int_{\Omega_e} \mathbf{G}^{\mathrm{T}} \mathbf{S} \mathbf{G} d\Omega. \tag{26}$$

The matrix $\mathbf{S}$ depends on the element's stresses. The stress vector $\sigma_\mathbf{e}$ is computed at the Gauss points, which provides enough accuracy for the proposed model. We acknowledge that zig-zag boundaries still exist in this method, and further stress estimation could be improved by using alternative techniques, such as the super convergent patch recovery. However, for the

buckling formulation, this did not show to be a problem using the TOBS method. The stress components are obtained for each element as

$$\sigma_{\mathbf{e}} = \left\{ \begin{array}{c} \sigma_x \\ \sigma_y \\ \tau_{xy} \end{array} \right\} = \mathbf{DBu}, \tag{27}$$

where $\mathbf{D}$ represents the element elasticity matrix (herein the 2D plane-stress elasticity matrix), $\mathbf{B}$ is the element strain-displacement matrix and $\mathbf{u}$ is the displacement vector. Once the stress vector is obtained, the stress matrix $\mathbf{S}$ can be obtained as

$$\mathbf{S} = \left[\begin{array}{cccc} \sigma_x & \tau_{xy} & 0 & 0 \\ \tau_{xy} & \sigma_y & 0 & 0 \\ 0 & 0 & \sigma_x & \tau_{xy} \\ 0 & 0 & \tau_{xy} & \sigma_y \end{array} \right]. \tag{28}$$

The matrix $\mathbf{G}$ in (26) denotes the shape function derivatives, and is expressed as

$$\mathbf{G} = \left[\begin{array}{cccccccc} N_{1,x} & 0 & N_{2,x} & 0 & N_{3,x} & 0 & N_{4,x} & 0 \\ N_{1,y} & 0 & N_{2,y} & 0 & N_{3,y} & 0 & N_{4,y} & 0 \\ 0 & N_{1,x} & 0 & N_{2,x} & 0 & N_{3,x} & 0 & N_{4,x} \\ 0 & N_{1,y} & 0 & N_{2,y} & 0 & N_{3,y} & 0 & N_{4,y} \end{array} \right]. \tag{29}$$

The stress stiffness matrix $(\mathbf{K}_\sigma)$ is assembled after each element stress stiffness matrix $(\mathbf{K}_\sigma^{(e)})$ is computed. The integration is computed using a numerical approach: Gauss quadrature. In this case, a discrete set of four Gauss points, two for each axis, is defined by each iteration loop i.

$$\mathbf{K}_\sigma^{(e)} = \sum_{i=1}^{4} \mathbf{G}_i^{\mathrm{T}} \mathbf{S}_i \mathbf{G}_i \tag{30}$$

The stress stiffness matrix $\mathbf{K}_\sigma$ is then assembled, and the eigenproblem 24 is then solved.

4 METHODOLOGY

4.1 Proposed formulation - buckling-constrained TO problem

The mathematical formulation of the compliance minimization problem of continuum structures with constraints on the material volume and the buckling load factor can be stated as:

$$
\begin{aligned}
\underset{\mathbf{x}}{\text{Minimize}} \quad & C(\mathbf{x}) = \mathbf{F}^{\mathrm{T}}\mathbf{u} = \mathbf{u}^{\mathrm{T}}\mathbf{Ku} \\
\text{Subject to} \quad & \mathbf{Ku} = \mathbf{F} \\
& V(\mathbf{x}) \leq \overline{V} \\
& \min_{i \in M} \lambda_i \geq \overline{\lambda} \\
& x_j \in [0,1]; \quad j = 1, ..., N_d,
\end{aligned}
\tag{31}
$$

where $\mathbf{x}$ is the design variable vector, $C(\mathbf{x})$ is the structural compliance, $\mathbf{u}$ and $\mathbf{F}$ are the global displacement and force vectors respectively, $\mathbf{K}$ is the global stiffness matrix. A set M of buckling modes are computed and the minimum buckling load factor, i.e. λ_1, is constrained by a lower bound $\overline{\lambda}$. $\overline{V}$ denotes the upper limit for the total material volume $V(\mathbf{x})$. Each design variable x_j can assume a void $\{0\}$ or solid $\{1\}$ state, and N_d is the total number of design variables.

Designs that fail to satisfy stability requirements are excluded from the feasible solution set by adopting such an explicit constraint for the buckling load factor. Theoretically, this value can represent different scenarios according to its magnitude: $\overline{\lambda} > 1$ denotes the case where the structure is under a safe stability performance, i.e. will not buckle. On the other hand, optimum designs are prone to buckling when $\overline{\lambda} \leq 1$ [18].

As performed in the TOBS method, the linearized objective function and constraints of the proposed topology optimization problem are obtained by the first order Taylor's approximation, which can be expressed for the iteration k as shown in Eq. (32):

$$
C(\mathbf{x}) \approx C(\mathbf{x}^k) + \frac{\partial C(\mathbf{x}^k)}{\partial x} \cdot \Delta \mathbf{x}^k + O(||\Delta \mathbf{x}^k||_2^2),
\tag{32a}
$$

$$
V(\mathbf{x}) = V(\mathbf{x}^k) + \frac{\partial V(\mathbf{x}^k)}{\partial x} \cdot \Delta \mathbf{x}^k
\tag{32b}
$$

$$
\lambda_1(\mathbf{x}) \approx \lambda_1(\mathbf{x}^k) + \frac{\partial \lambda_1(\mathbf{x}^k)}{\partial x} \cdot \Delta \mathbf{x}^k + O(||\Delta \mathbf{x}^k||_2^2).
\tag{32c}
$$

Employing the sequential linear approximation from Eq. (32), the original problem - see (31) - is then solved by TOBS as subotimization problems expressed by

$$\begin{aligned}
\underset{\Delta \mathbf{x}^k}{\text{Minimize}} \quad & \frac{\partial C(\mathbf{x}^k)}{\partial x} \cdot \Delta \mathbf{x}^k \\
\text{Subject to} \quad & \frac{\partial V(\mathbf{x}^k)}{\partial x} \cdot \Delta \mathbf{x}^k \leq \bar{V} - V(\mathbf{x}^k) := \Delta V^k \\
& \frac{\partial \lambda_1(\mathbf{x}^k)}{\partial x} \cdot \Delta \mathbf{x}^k \geq \bar{\lambda} - \lambda_1(\mathbf{x}^k) := \Delta \lambda_1^k \\
& \Delta \mathbf{x}_j \in \{-x_j, 1 - x_j\}, \quad j \in [1, N_d].
\end{aligned}$$

(33)

Once the optimum change $\Delta \mathbf{x}^k$ is obtained, the design variables are updated as $\mathbf{x}^{k+1} = \mathbf{x}^k + \Delta \mathbf{x}^k$.

In order to keep the constraints feasible at each each iteration, the TOBS method adopts a relaxation parameter ϵ that updates the upper/lower bounds depending on the constraint values $V(\mathbf{x}^k)$ and $\lambda_1(\mathbf{x}^k)$. For instance, the volume constraint, bounded by $\Delta V^k = \bar{V} - V(\mathbf{x}^k)$, might become unfeasible at iteration k. To avoid this issue, a subproblem is defined so that the constraint bounds are properly updated:

$$\Delta V^k = \begin{cases}
-\epsilon_v V(\mathbf{x}^k) & : \overline{V} < (1 - \epsilon_v) V(\mathbf{x}^k), \\
\overline{V} - V(\mathbf{x}^k) & : \overline{V} \in [(1 - \epsilon_v) V(\mathbf{x}^k), (1 + \epsilon_v) V(\mathbf{x}^k)], \\
\epsilon_v V(\mathbf{x}^k) & : \overline{V} > (1 + \epsilon_v) V(\mathbf{x}^k),
\end{cases}$$

(34)

where ϵ_v expresses the relaxation parameter corresponding to the volume constraint. Similarly, the same procedure is adopted for the buckling constraint, in which a relaxation parameter ϵ_b is defined. When the volume constraint $V(\mathbf{x}^k)$ approaches $\overline{V}$ from above with a significant difference, the upper bound is defined as $-\epsilon_v V(\mathbf{x}^k)$, so that $V(\mathbf{x}^k)$ gradually decreases towards the upper limit according to the fraction specified by ϵ_v.

4.1.1 Sensitivity analysis

As the TOBS method is a gradient-based approach, the derivatives of the objective function and the constraints are to be computed for design variable updating. Element sensitivities measure the change in the objective/constraint functions when an element changes its state from void to solid. The gradient is fundamental for the optimization solver to properly update the design variables and leads to the optimum solution.

If a design-dependent load is being applied over the structure e.g. pressure loading, the change in the fluid-solid coupling matrix $\mathbf{L}_{fs}$ influences the compliance sensitivity based on the design variable x_j removal. The equation that evaluates the compliance sensitivity analysis for such problems is shown in (35):

$$\frac{\partial C}{\partial x_j} \approx -\frac{1}{2} \mathbf{u}_j^{\mathrm{T}} \mathbf{K}_j^e \mathbf{u}_j + \mathbf{u}_j^{\mathrm{T}} \Delta \mathbf{L}_{fs} \mathbf{P}_{fj},$$

(35)

where $\mathbf{u}_j$ and $\mathbf{K}_j^e$ are the displacement vector and the stiffness matrix corresponding to element j, $\mathbf{P}_{fj}$ is the fluid pressure in the fluid finite element which shares its boundary with the solid finite element j, and $\Delta \mathbf{L}_{fs} = \mathbf{L}_{fs}^* - \mathbf{L}_{fs}$ is a semi-analytical sensitivity of the fluid-solid

coupling matrix, where $\mathbf{L}_{fs}$ and $\mathbf{L}_{fs}^*$ are the fluid-solid coupling matrices obtained before and after changing the solid element j to fluid [82].

- Volume sensitivity

The sensitivity of the volume function depends on the structural volume V which can be expressed as

$$V = \sum_{j=1}^{N_d} x_j V_j, \tag{36}$$

where x_j is the binary design variable for the element j, V_j is the volume of finite element j and N_d is the total number of design variables. Therefore, the derivative of V with respect to the design variable x_j is equivalent to the volume of the element j.

$$\frac{\partial V}{\partial x_j} = V_j. \tag{37}$$

- Buckling load factor sensitivity

According to Rodrigues et al. (1995) [101], the buckling sensitivity analysis is calculated for an eigenvalue λ_i with respect to the design variable x_j as

$$\frac{\partial \lambda_i}{\partial x_j} \approx \varphi_i^{\mathrm{T}} \left(\frac{\partial \mathbf{K}}{\partial x_j} + \lambda_i \frac{\partial \mathbf{K}_\sigma}{\partial x_j} \right) \varphi_i - \lambda_i \mathbf{v}^{\mathrm{T}} \frac{\partial \mathbf{K}}{\partial x_j} \mathbf{u}, \tag{38}$$

where $\mathbf{v}$ is obtained by solving the adjoint system

$$\mathbf{K}\mathbf{v} = \varphi_i^{\mathrm{T}} \left(\frac{\partial \mathbf{K}_\sigma}{\partial \mathbf{u}} \right) \varphi_i. \tag{39}$$

The second term on the right side of Eq. 38, also named the adjoint term, is believed to be negligible according to some researchers seeking to reduce computation cost [102]. However, Ferrari and Sigmund (2018) affirms that omitting this term could lead to inconsistent sensitivities, generating questionable designs [14].

As seen in Eq. 38 and 39, the derivatives of the stress stiffness matrix $\mathbf{K}_\sigma$ with respect to the design variable x_j are required along with the displacement vector $\mathbf{u}$. The sensitivity of the stress stiffness matrix $\mathbf{K}_\sigma$ is obtained as

$$\frac{\partial \mathbf{K}_\sigma}{\partial x_j} = \sum_{j=1}^{N_d} \frac{\partial \mathbf{K}_\sigma^{(e)}}{\partial x_j} = \sum_{j=1}^{N_d} (\mathbf{G}^{(e)\mathrm{T}}) \frac{\partial \mathbf{S}^{(e)}}{\partial x_j} \mathbf{G}^{(e)}. \tag{40}$$

As defined in 28, $\mathbf{S}$ consists of the element's stress components. Therefore, its sensitivity can be expressed as

$$\frac{\partial \mathbf{S}^{(e)}}{\partial x_j} = \mathbf{S} \left(\left[\frac{\partial \sigma^{(e)}}{\partial x_j} \right] \right). \tag{41}$$

The derivatives of the stress vector σ with respect to the design variable x_j will be zero for all elements different than x_j. It occurs since the element elasticity matrix $\mathbf{D}$ is explicilty

dependent on x_j, and it is present in the stress equation - see Eq. 27. Thus, the sum required to obtain $\frac{\partial \mathbf{K}_\sigma}{\partial x_j}$ can be reduced to the element stress stiffness matrix $\mathbf{K}_\sigma^{(\mathbf{e})}$ only.

$$\frac{\partial \mathbf{K}_\sigma}{\partial x_j} = \mathbf{K}_\sigma^{(\mathbf{e})}. \tag{42}$$

On the other hand, to calculate the adjoint term $\mathbf{v}$ - see Eq. 39 -, the stress stiffness matrix is differentiated with respect to the displacement vector $\mathbf{u}$.

$$\frac{\partial \mathbf{K}_\sigma}{\partial \mathbf{u}} = \left\{ \frac{\partial \mathbf{K}_\sigma}{\partial u_1}, \frac{\partial \mathbf{K}_\sigma}{\partial u_2}, \dots, \frac{\partial \mathbf{K}_\sigma}{\partial u_d} \right\}^{\mathrm{T}}, \tag{43}$$

where d is the number of degrees of freedom of the structure. As shown in Eq. 27, the displacement vector of the element j is used to compute the stress components, and later to obtain the stress stiffness matrix. For instance, the derivatives of the stress tensor of element j with respect to displacement component u_1 is computed as:

$$\frac{\partial \sigma_j}{\partial u_1} = \mathbf{DB} \left\{ \frac{\partial u_1}{\partial u_1}, \frac{\partial u_2}{\partial u_1}, \dots, \frac{\partial u_j}{\partial u_1} \right\}^{\mathrm{T}} = \mathbf{DB}\{1, 0, \dots, 0\}^{\mathrm{T}}, \tag{44}$$

where u_j represents the displacement component related to the 8th degree of freedom of the element j. In order to save computational time, the stress stiffness matrix sensitivity - see Eq. 43 - is assembled considering only active degrees of freedom of the element j. This is adopted because the displacement vector derivatives $\frac{\partial \mathbf{u}_j}{\partial u_i}$ is null - and so is $\frac{\partial \mathbf{K}_\sigma^{(\mathbf{j})}}{\partial u_i}$ - if $u_i \notin \mathbf{u}_j$.

4.2 Computational procedure

Based on the previous theoretical concepts regarding topology optimization, buckling mechanism and pressure loading, this work proposed the use of the TOBS Method to develop such optimization simulations. Compared to the conventional methodology, the stability parameter has been added to the compliance minimization under volume constraint, besides the adoption of binary variables. The implementation has been developed using the commercial software MATLAB. The flowchart exposed in Figure 10 illustrates the iteration procedure algorithm divided into seven main steps, proposed for the solution of the topology optimization problem. Each step is properly described in the following subtopics.

4.2.1 Step 1: Definition of the problem model and optimization parameters

Initially, the optimization problem must be defined according to the material information, design domain, type of loading and boundary conditions. It is provided the Young's Modulus, Poisson's ratio and structure dimensions. The domain is then discretized into equally-sized square four-node elements. The number of elements depends on the final purpose of the simulation: refined meshes usually perform in a more realistic way, but require a high computational cost, especially when an eigenvalue problem is solved at each iteration. This trade-off usually depends on each problem complexity and the computational capacity available.

Besides the optimization problem data, the optimization solver requires certain inputs to determine the technical features of the iteration process. These parameters are related to the
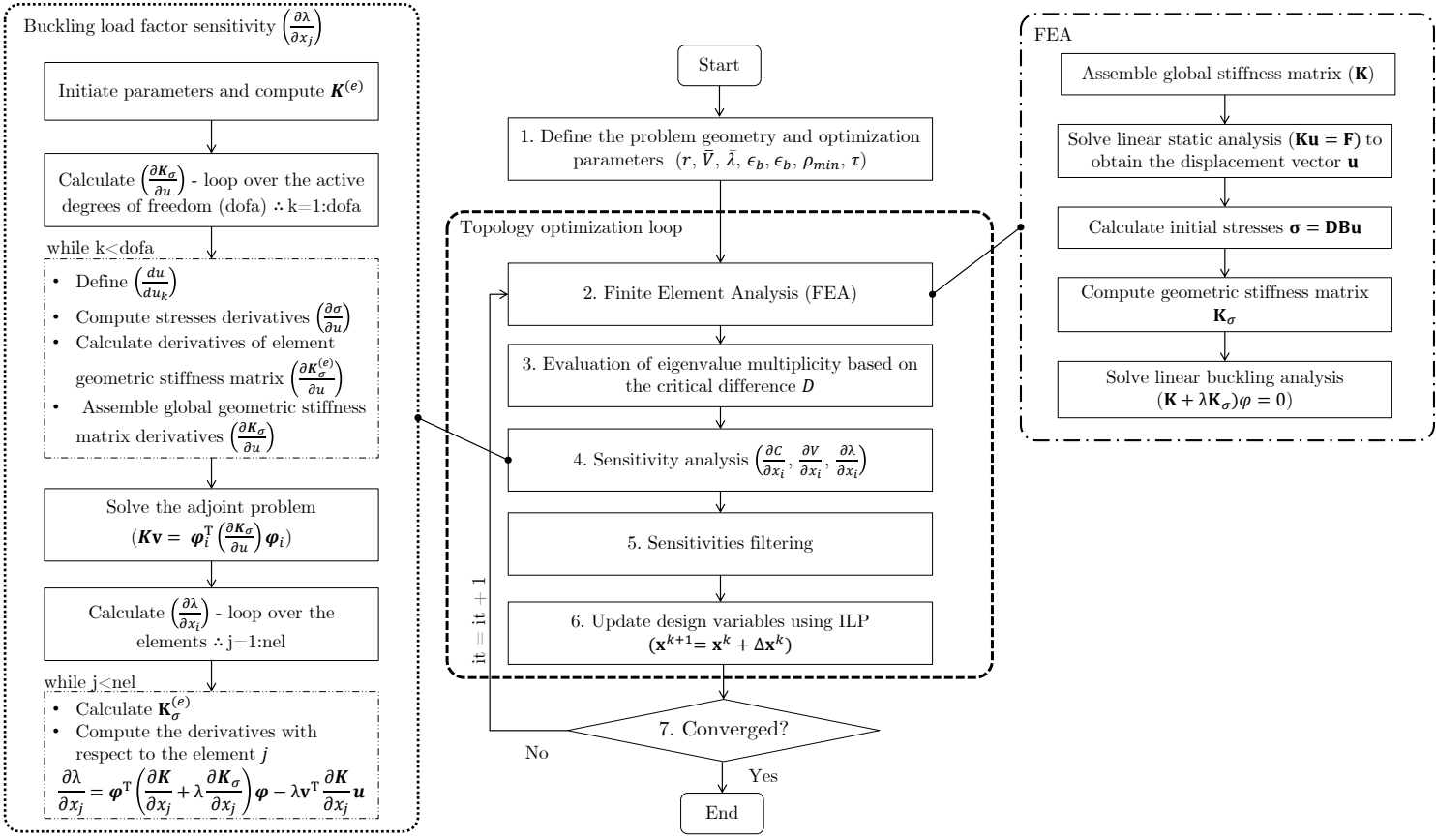
Figure 10: Flowchart of the proposed methodology algorithm.

final design constraints - both for volume $(\overline{V})$ and buckling load factor $(\overline{\lambda})$ - and to specific data, essential throughout the optimization process. The filter radius - r -, for example, is fundamental to avoid the checkerboard problem and it also influences the bars' thickness. This parameter will be further explained in Step 4.

The pace on which the constraint value $(\lambda_1$ and $V(x))$ reaches the defined bound $(\overline{\lambda}$ and $\overline{V})$ is determined by the ϵ's. This parameter is represented by ϵ and expresses the move limits for the constraint functions. Thus, it has to be chosen individually for each constraint - volume (ϵ_v) and buckling (ϵ_b) -, as well as has to be selected in order to prevent the design to change drastically between iterations. The hard-kill approach is adopted to represent the void regions. Such elements are ignored from the Finite Element Analysis in order to preserve the binary nature of the problem and to spare computational resources.

The convergence criteria is also a determinant input for the optimization performance. The symbol τ defines the limit that determines the optimization completion, and is also dependent on the user's purpose on the optimum design. The convergence criteria will be covered in detail in Step 7.

4.2.2   Step 2: Finite Element Analysis

The FE analysis is performed to obtain the structural performance from the initial full domain until the converged design, providing the required input for the optimizer and evaluating

the structure's at each iteration k. As the solid interface might change throughout the optimization process, specific algorithms are implemented to track the boundary and update the pressure loading interaction. In this work, this process is developed by the fluid flooding technique, as first proposed by Chen and Kikuchi (2001) [75]. For each iteration, the fluid region is updated until their corresponding elements are completely in contact with the structure, as shown in Figure 11 [7].
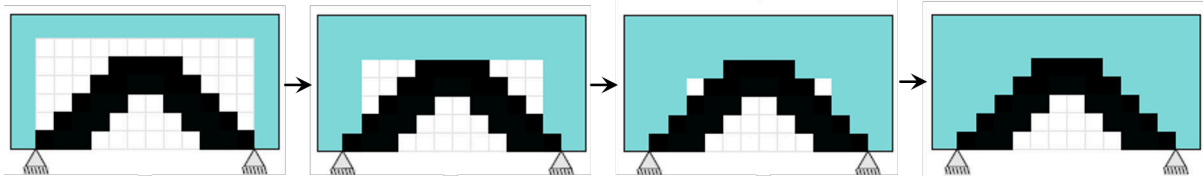
Figure 11: Fluid flooding scheme, as illustrated by Picelli (2015) [7]

The Finite Element Analysis FEA is detailed in Fig. 10. First, the equilibrium equation is computed once the global stiffness matrix is assembled. The displacement vector is then obtained, followed by the stresses calculation and the stress stiffness matrix assembly. Lastly, the linear eigenproblem is solved, obtaining the buckling modes and its corresponding buckling load factors. It is known that the computational cost exponentially increases as the mesh size gets finer [90, 103]. This context represents a challenge since complex study cases usually require a significant fine mesh to obtain a suitable result - and that might be unfeasible, depending on the available resources.

4.2.3 Step 3: Evaluation of eigenvalue multiplicity

A common issue present in optimization problems that consider single eigenvalue constraint is the occurrence of multiple eigenvalues. In this case, two or more buckling modes share the same buckling load factor, and this fact can jeopardize the convergence process by affecting the eigenvalue sensitivity analysis. Previous works have discussed that multiple eigenvalues are not differentiable using the single eigenvalue sensitivity approach - Eq. (38) [100, 104]. An understandable explanation for this problem can be seen when Eq. (38) is analysed: when a single eigenvalue λ_1 is differentiated with respect to the design variable x_j, its corresponding buckling mode φ_1 also contributes to the sensitivity analysis. However, if a different eigenmode shares the same value of the eigenvalue - e.g. $\lambda_2 = \lambda_1$ -, its contribution by φ_2 is being ignored and the overall sensitivity efficiency becomes affected. This method usually causes poor convergence scenarios or poor local minima solutions.

Therefore, after each set of eigenpairs (λ_i, φ_i) is computed, the difference between the eigenvalues must be determined in order to evaluate if a single buckling load sensitivity analysis is suitable or not. As the linear buckling analysis represents an approximation, it is desirable to define a critical difference that determines the multiplicity occurrence. In this work, this parameter is defined as D, and expresses the critical difference of each eigenvalue $\lambda_2, \lambda_3, ..., \lambda_i$ regarding λ_1. If this difference is lower than D, a proper methodology is applied to consider n buckling modes inside the sensitivity analysis - see Step 4. The parameter D was established according to a trial and error analysis, comparing different values. We noticed that values lower than 10% presents little influence on the convergence and a reasonable oscillation by including

and neglecting the eigenmultiplicity among iterations. On the other hand, high values of D considers the multiplicity of buckling modes that do not play a significant role in the convergence process. Therefore, for the proposed problems, the assigned critical difference for multiplicity was 20%.

This verification is allocated in the variable $BuckDiff_i$ and calculates, in percentage, the difference of buckling mode i compared to the lowest buckling mode λ_1.

$$BuckDiff_i = \left(\frac{\lambda_i - \lambda_1}{\lambda_1} \right) \cdot 100, \qquad \forall i \in M. \tag{45}$$

The variation is then compared to the critical difference parameter, and the modes whose difference is lower than D are allocated in set K.

$$\text{if} \quad BuckDiff_i \leq D, \quad i \in K. \tag{46}$$

4.2.4   Step 4: Sensitivity analysis

Once the FEA and the eigenvalue multiplicity evaluation have been completed, the sensitivity analysis is performed for the functions involved in the optimization problem. As previously explained, this information is fundamental for the correct and efficient element update stage. The sensitivity analysis regarding the compliance and volume functions are well-known from the literature and relatively easy to implement - expressed by Eq. 35 and 37, respectively. Recent works have discussed and improved the efficiency to compute buckling sensitivities [15, 28], but this analysis (see Eq. 38) still presents a non-trivial computational routine and potential challenges inherent to the nature of the problem. One of the issues that impacts on the buckling sensitivity is the multiplicity of eigenvalues. This problem has been widely discussed [104–106] and a few methods have been developed to deal with it.

This work proposes a methodology that has been discussed by Xie and Steven (1997) [107], and computes the sensitivity analysis of the buckling load factor considering n critical buckling modes according to a defined difference - D - regarding the lowest one (λ_1). In practice, the purpose is to add, into the sensitivity calculation, the buckling modes with eigenvalues whose difference from λ_1 is small enough to be considered critical. If that is the case, the sensitivity turns out to be computed as the average mean of all crucial buckling modes, present in set K.

If no buckling load factor is lower than the defined difference, only the first buckling mode and its corresponding eigenvalue are used for the sensitivity analysis. If two or more buckling modes are critical, their arithmetic average is computed and assigned to the final buckling sensitivities $\frac{\partial \lambda_f}{\partial x_j}$:

$$\frac{\partial \lambda_f}{\partial x_j} = \frac{\dfrac{\partial \lambda_1}{\partial x_j} + \sum_{i=1}^{K} \dfrac{\partial \lambda_{i+1}}{\partial x_j}}{1 + K}. \tag{47}$$

4.2.5   Step 5: Filtering

A standard spatial filtering [108] technique is applied to the compliance and the buckling sensitivities, seeking to prevent numerical issues, such as the checkerboard problem. An

advantage of using filtering in the TOBS method is that no projection methods are required. According to Huand and Xie (2007) [81] methodology, the filtered sensitivities can be computed for an element j based on the weighted sensitivities of the neighbour elements defined by a radius r. The filtered sensitivity field $\dfrac{\widetilde{\partial f}}{\partial x_j}$ for an element j is calculated as:

$$\frac{\widetilde{\partial f}}{\partial x_j} = \frac{1}{\sum_{m \in N_m} H_{jm}} \sum_{m \in N_m} H_{jm} \frac{\partial f}{\partial x_m} \tag{48}$$

where the elements m which center-to-center distance is smaller than r is allocated in the set N_m. H_{jm} is a weight factor given as:

$$H_{jm} = \max(0, r - \text{dist}(x_j, x_m)) \tag{49}$$

The idea is that the defined weights allow the closer elements to contribute larger to the filtered sensitivities of the reference element j, when compared to farther ones. The filtering scheme is illustrated, for elements 1 and 2, in Figure 12:
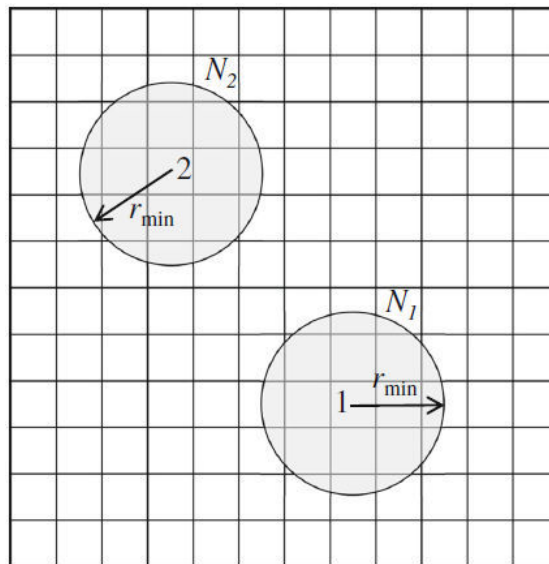
Figure 12: Filter radius scheme considered for elements 1 and 2 [8].

An example has been developed to observe the effect of the filtering technique on the final designs. A topology optimization problem of volume minimization under compliance constraint was adopted. The example model is shown in Figure 13 (a). Three different scenarios were simulated: (b) no filtering, (c) filtering with $r = 3$ elements and (d) filtering with $r = 10$ elements - see Figure 13.

The final design (b), where no filtering was used, represents a case where the checkerboard problem occurs. The absence of filtering allows the solver to generate bars or regions connected only by the elements' nodes. This pattern creates a numerically induced, artificially high stiffness. On the other hand, the filtering technique promotes the generation of solid bars/regions - (c) and (d). Regarding the models in which the filtering was used, it can be observed the effect over the bars' thickness, and the overall final topology. Smaller r allows the solver to create thinner bars - and the opposite is noticed for larger filter radius. Thus, the filtering turns out

(a) Example model

(b) $r = 0.00$

(c) $r = 0.30$ (3 elements)

(d) $r = 1.00$ (10 elements)
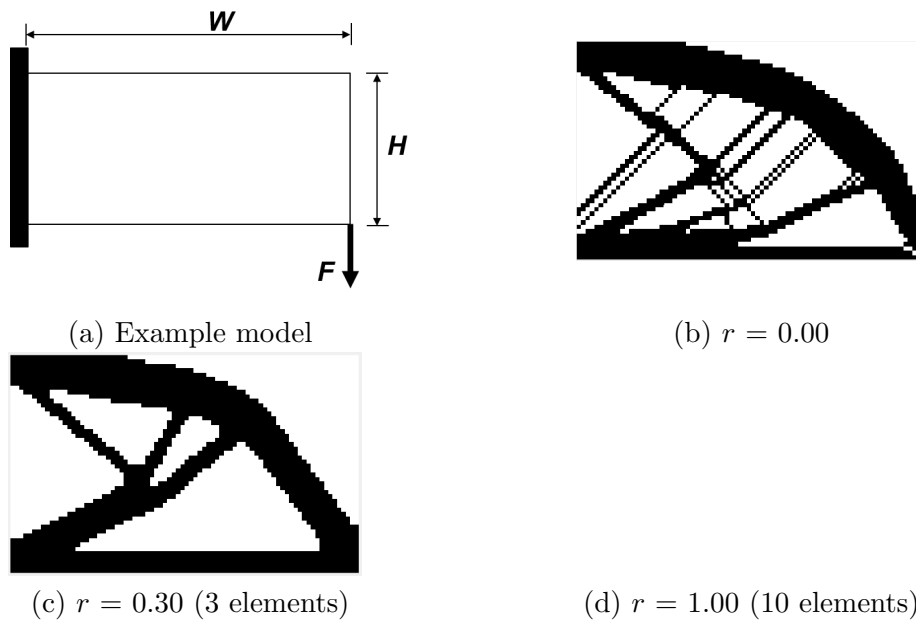
Figure 13: Filtering influence observed for different r applied to an example model.

to be a tool of influencing the final topology and its elements' configuration.

4.2.6 Step 6: Design variables update

After the filtering information has been provided to the optimization solver, the integer linear problem - Eq. 33 - is solved and the design variable x is updated considering the optimum change Δx as

$$x^{k+1} = x^k + \Delta x^k. \tag{50}$$

The variable change will define which elements will become, remain or return to be solid 1 and void 0, based on the criteria design to avoid abrupt changes between iterations.

4.2.7 Step 7: Convergence criteria

The optimization iteration process is concluded when the final topology respects the determined criteria and then its convergence is assumed. The methodology for this stage was based on Huang and Xie (2007) [81], and defines that besides the constraint functions fulfillment, the design must meet a stable compliance for at least $2N$ iterations. The error - Eq. 51 - that computes the objective function difference must be lower than the defined convergence parameter τ.

$$error = \frac{|\sum_{i=1}^{N}(C_{k-i+1} - C_{k-N-i+1})|}{\sum_{i=1}^{N} C_{k-i+1}} \leq \tau \tag{51}$$

where k is the current iteration number, τ is the convergence parameter - error acceptance - and N is an integral number which is usually selected as 5. Once all the convergence requirements have been fulfilled, the final topology is plotted and saved as the optimum solution.

5 RESULTS AND DISCUSSIONS

5.1 Linear buckling analysis verification

In order to assure the code's accuracy, a few numerical examples have been tested and verified with analytical methods. According to Euler's equation, the critical load (F_{cr}) on the column, just before it begins to buckle, with fixed and free ends, is:

$$F_{cr} = \frac{\pi^2 E I}{(2L)^2}, \tag{52}$$

where E is the modulus of elasticity for the material, I is the minimum moment of inertia for the column's cross-sectional area and L is the length of the column. An example - see Figure 14 - with the following properties was used:

- cross-sectional area: 1x1 m;

- $L = 10$ m;

- $E = 1$ Pa;

- $I = \dfrac{1}{12}$ m^4;

- point load (F) = $1 \cdot 10^{-3}$ N.

Figure 14: Column model used for linear buckling verification.

5.1.1 Analytical solution

According to Euler's equation, Eq. (52), the column's critical buckling force for the analytical approach is:

$$F_{cr} = \frac{\pi^2 \cdot 1 \cdot \left(\dfrac{1}{12}\right)}{(2 \cdot 10)^2} \qquad \Rightarrow F_{cr} = 2.056 \cdot 10^{-3} \text{ N}. \tag{53}$$

To obtain the corresponding buckling load factor (λ_1), Eq. (25) is evaluated, where

$$\lambda_1 = \frac{F_{cr}}{F_0} \qquad \Rightarrow \lambda_1 = \frac{2.056 \cdot 10^{-3} \text{ N}}{1 \cdot 10^{-3} \text{ N}} \qquad \Rightarrow \lambda_1 = 2.056. \tag{54}$$

5.1.2 Numerical solution and verification

For the numerical solution, three different finite element discretizations were used - 2x20, 4x40 and 10x100 -, aiming to verify the mesh refinement effect on the buckling load factor. The results compilation are shown in Table 1.

As observed in Table 1, the numerical solution achieved the first buckling load factor close to the analytical approach. Considering different meshes, the error decreased as the mesh got finer. The results showed that the linear buckling implementation using the Finite Element Method was successful.

Table 1: Linear buckling solved by the Finite Element Method for different discretization setups.

FE Discretization	1st Buckling mode	1st Buckling load factor	Absolute error compared to analytical solution
2×20		2.294	11.58%
4×40		2.105	2.38%
10×100		2.052	0.19%
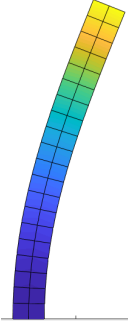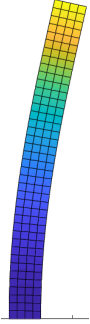
5.2 Numerical examples

In order to apply the proposed methodology, three well-known cases from the literature explore different perspectives concerning the buckling constraint and pressure loadings. The first example presents a column-like structure, which is a benchmark problem for buckling-constrained TO formulations. The pressure loading case is included in the second example, where an arch-like structure is analyzed. The piston-head model composes the third study case, and besides the fluid pressure, the boundary condition - expressed by the support type - is investigated regarding its influence on the structure's overall stability. All examples adopt non-dimensional parameters. The compliance design is initially developed and used as a reference, mainly to determine the buckling constraint starting point - since one of this work's purpose is to

obtain a more stable solution when compared to the classic approach. The assigned convergence criteria is $\tau = 0.001$ for all problems. The parameter ϵ_v is set to 0.005, and ϵ_b, which is less intuitive, is chosen individually for each example based on numerical experience. We consider $\beta = 0.05$.

5.2.1 Example 1

In this example, the buckling mechanism is considered as a constraint for a column-like structure optimization. A similar model has been studied by Gao and Ma (2015) [100], and its geometry properties are shown in Figure 15(a). The structure is subjected to a distributed centered load $q = 0.12$ at the top with a width of $d = 2/3$ and has its bottom edge clamped. The initial full domain has a rectangular shape with dimensions of 20x40 and unit thickness. The domain is discretized into 60×120 quadrilateral finite elements. For the material properties, we consider the Young's Modulus of $E = 1$ and the Poisson ratio is $\nu = 0.30$. The volume constraint defines a final fraction of 0.35 of the full design domain. The relaxation parameter related to the volume constraint is $\epsilon_v = 0.005$ and to the buckling constraint is $\epsilon_v = 1 \cdot 10^{-7}$. The filter radius is set to $r = 2$ elements. Different buckling constraints $(\overline{\lambda})$ have been defined seeking to investigate the buckling influence on the final topology.

(a) Design Problem

(b) $\overline{\lambda} = 0$
$\lambda_1 = 0.62$
$C = 4.34 \cdot 10^{-2}$

(c) $\overline{\lambda} = 0.80$
$\lambda_1 = 0.81$
$C = 4.40 \cdot 10^{-2}$

(d) $\overline{\lambda} = 1.00$
$\lambda_1 = 1.02$
$C = 4.38 \cdot 10^{-2}$

(e) $\overline{\lambda} = 1.20$
$\lambda_1 = 1.23$
$C = 4.41 \cdot 10^{-2}$

(f) $\overline{\lambda} = 1.40$
$\lambda_1 = 1.40$
$C = 4.46 \cdot 10^{-2}$

(g) $\overline{\lambda} = 1.60$
$\lambda_1 = 1.61$
$C = 4.54 \cdot 10^{-2}$

(h) $\overline{\lambda} = 1.80$
$\lambda_1 = 1.84$
$C = 4.67 \cdot 10^{-2}$

(i) $\overline{\lambda} = 2.00$
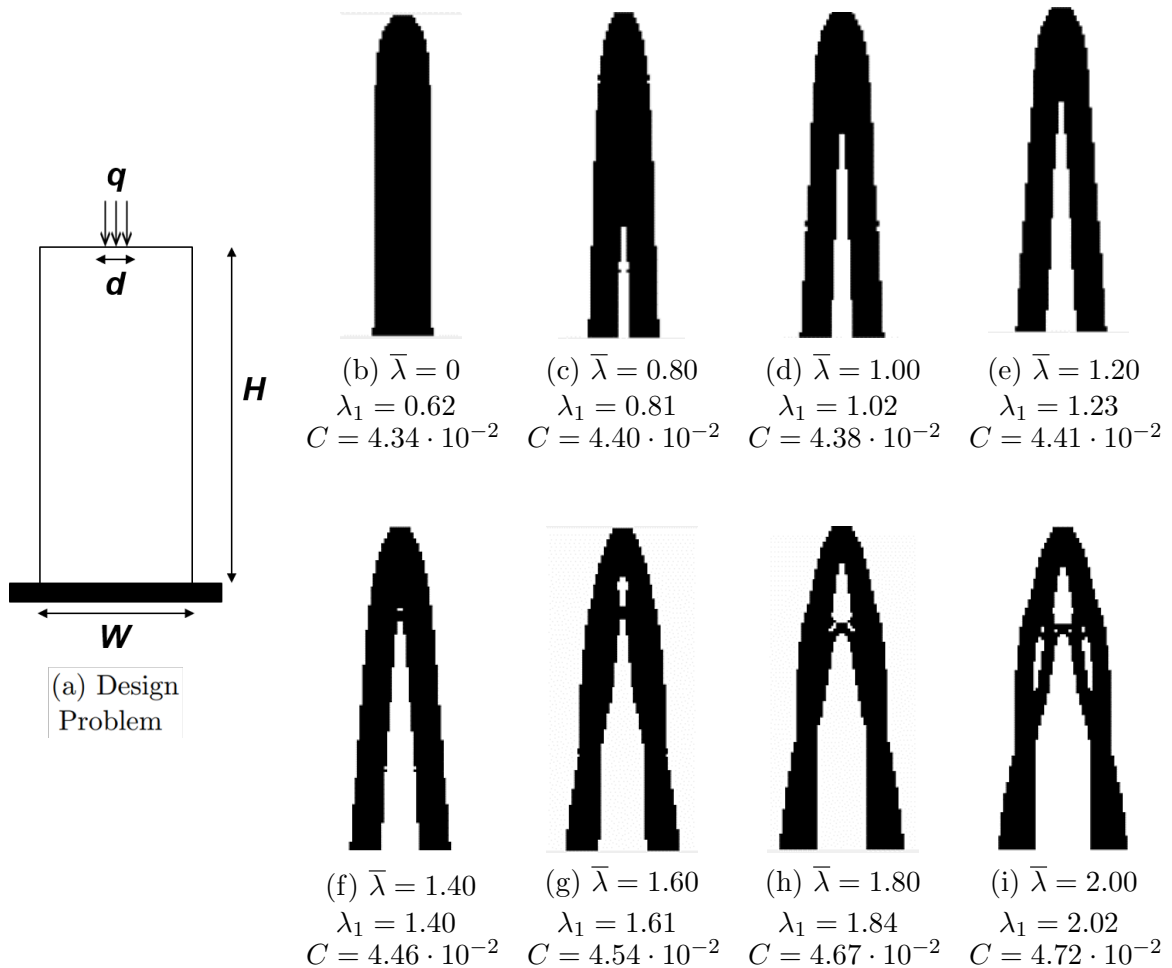$\lambda_1 = 2.02$
$C = 4.72 \cdot 10^{-2}$

Figure 15: Results compilation of Example 1.

As a baseline solution, the conventional optimization set up - compliance minimization under

volume constraint - is shown in Figure 15 (b) - and presents a buckling load factor of 0.62. Based on that, the algorithm which considers buckling has been solved for constrained buckling load factors from 0.80 to 2.00, with a step of 0.2. The optimized topologies are shown in Figure 15 (c)-(i).

Unlike the load path transfer topology observed for the stiffness maximization problem - see Fig. 15 (b) -, the stability constraint requires the column-like structure to split into two main bars, aiming to enlarge the support base and providing a more stable design - Figure 15 (c)-(e). From $\overline{\lambda} = 1.4$ onwards, an inner bar connecting the two inclined columns becomes crucial for the structural stability. A more complex design is achieved for $\overline{\lambda} = 2.0$, where intermediate voids are created, dividing the thick structure elements.

Figure 16 presents the optimization history for the compliance and volume values for the $\overline{\lambda} = 1.6$ model and its intermediate designs. Since the initial design domain is composed by a full solid rectangle area, the compliance increases as the material is removed to achieve the volume constrained. For this example, the eigenvalue multiplicity plays an important role for the optimization convergence. As the buckling constraint increases and generates more complex solutions, composed by slender members, the second buckling mode becomes critical as well. This fact can be observed in Figure 17, where the progress of the three first buckling load factors are plotted until convergence for the model $\overline{\lambda} = 1.6$.
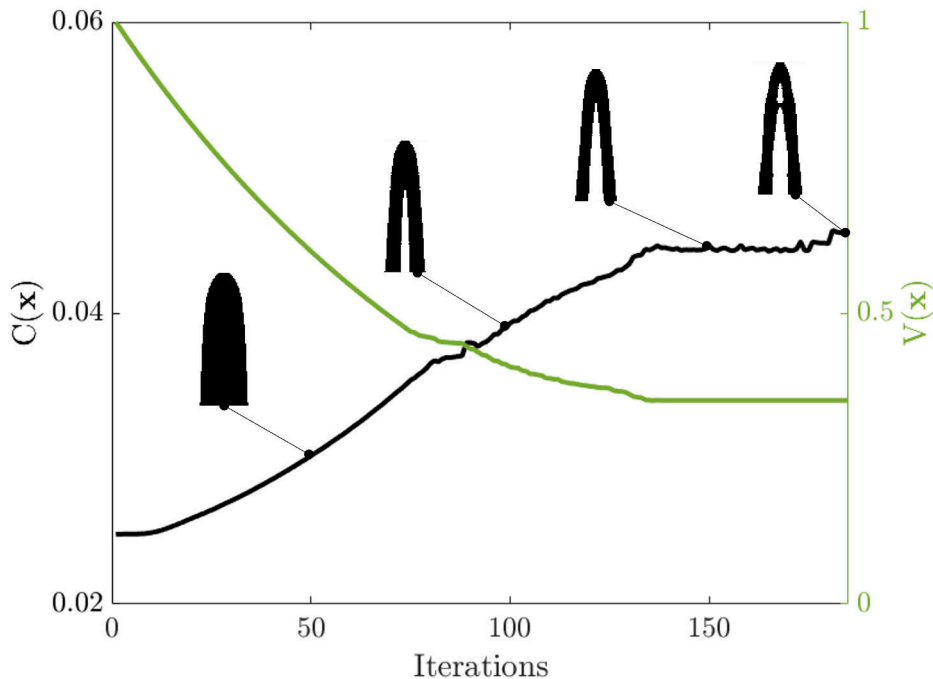
Figure 16: Optimization history for the compliance and volume functions - column structure with $\overline{\lambda} = 1.6$.

Figure 17 illustrates the importance of considering multiple buckling modes inside the optimization problem, especially regarding the design convergence. From iteration 130 on, the eigenvalue multiplicity strategy starts to actively influence the optimization solver by including both 1st and 2nd buckling modes inside the sensitivity analysis. It is observed that the similar buckling load factors values occur until the convergence - around iteration 170 -, confirming the significance of this phenomenon for stability-based optimization problems. As a matter of fact,
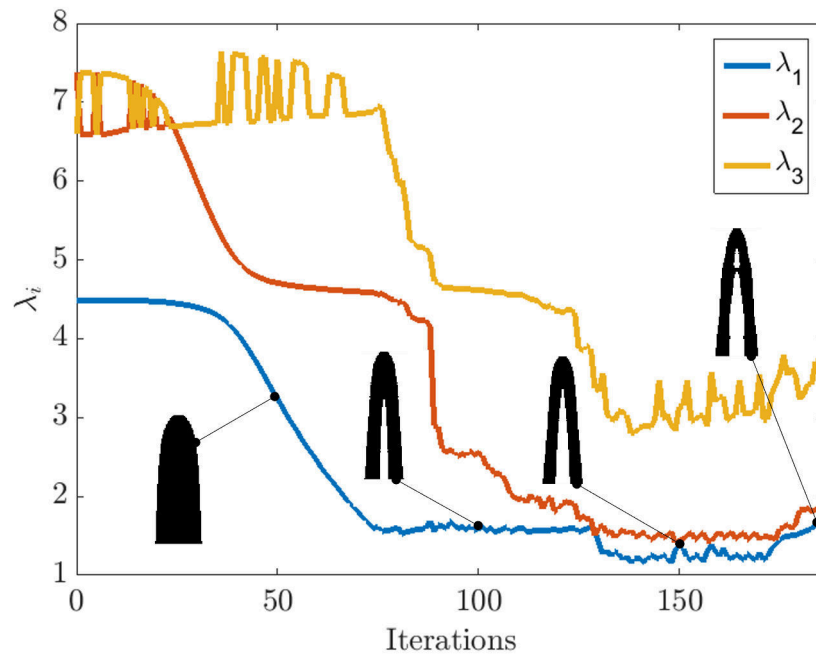
Figure 17: Optimization history for the first three buckling load factors - column structure with $\overline{\lambda} = 1.6$.

the algorithm that only considers the lowest buckling load factor information has been applied for this example and it was not able to achieve a λ_1 higher than 1.41 as a final solution.

(a) Optimum design for $\overline{\lambda} = 1.6$

(b) 1st buckling mode

(c) 2nd buckling mode
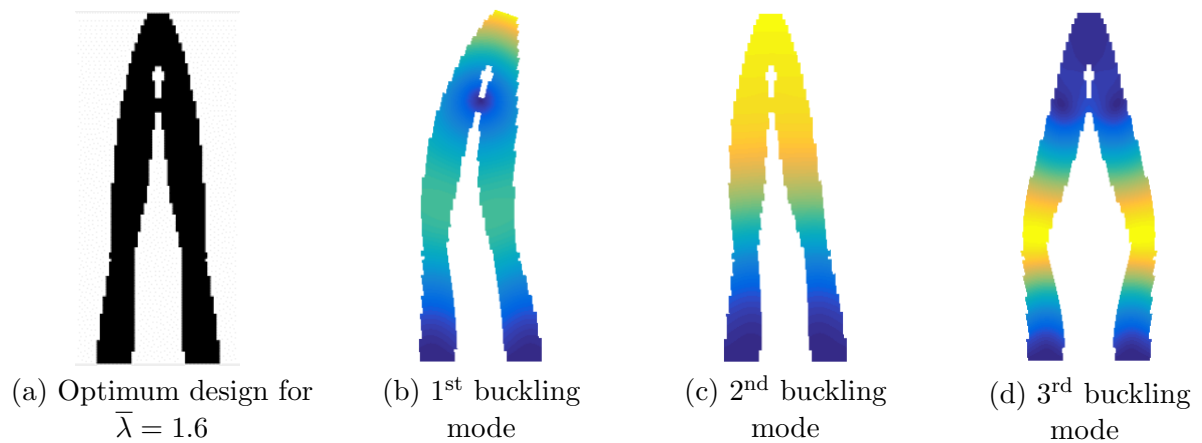
(d) 3rd buckling mode

Figure 18: Final topology for $\overline{\lambda} = 1.6$ and its three first buckling modes.

Figure 18 presents the first three buckling modes for the final design for $\overline{\lambda} = 1.6$. In a practical view, when only the lowest buckling load factor is constrained, higher buckling modes - representing different deformation settings - might become critical throughout the optimization process, and that is the key point of evaluating and considering this phenomenon inside the sensitivity analysis. Thus, the optimizer receives the appropriate information regarding where to strengthen in order to achieve an overall stability improvement.

The optimized designs obtained for the column under compression - Fig. 15 - using the proposed methodology presented similar results with those discussed by Gao and Ma (2015) [18]. Their work shared two main points of our findings: the inner bar was also fundamental for the solutions of higher buckling load factor constraints and the multimode sensitivity analysis was

crucial to circumvent the bimodal phenomenon observed in the final solutions. This reference verifies a novel application of the TOBS method considering a buckling-constrained problem and provides important insights for further investigations of pressure loaded problems that will be discussed in the following examples.

- TOBS parameters analysis: ϵ_b, ϵ_v and β

An investigation on the TOBS parameters has been developed in order to verify the solver's sensitivity to changes on the adopted parameters. The relaxation variable ϵ, which defines the move limits for the constraint functions, has been defined as $\epsilon_v = 0.005$ for the volume and $\epsilon_b = 1 \cdot 10^{-7}$ for the buckling constraint of Example 1. It has been noticed that small changes on ϵ_v impacts on the overall optimization pace on which the solver converges to the optimum solution. Higher values of ϵ_v allows a faster convergence by faster material removal.

Figure 19 illustrates this effect by displaying the optimization history for the volume function and their final solutions considering three different values for ϵ_v, based on a volume constraint of $\overline{V} = 0.35$. The lowest value $\epsilon_v = 0.0025$ required 236 iterations for convergence, while $\epsilon_v = 0.005$ and $\epsilon_v = 0.01$ demanded 124 and 91 iterations, respectively. Although the convergence process takes longer for lower ϵ_v values, it can be seen that a slightly better local minima could be achieved for the $\epsilon_v = 0.0025$ in terms of stiffness and stability parameters when compared to higher move limits. It is also worth-mentioning that the optimizer fails to find a feasible solution when ϵ_v is too high; for this example, $\epsilon_v > 0.01$ determined a critical value for this parameter where no optimum integer solution of the subproblem of the Eq. 33. This phenomenon could be influenced by the buckling constraint, which strives to move towards the lower bound if large move limits are adopted.

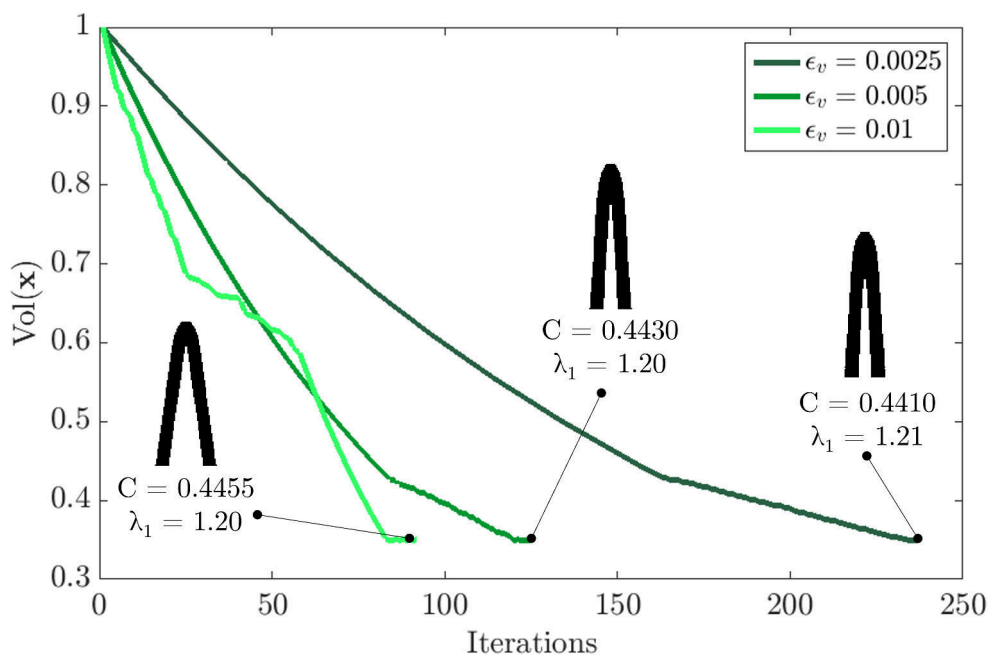Figure 19: Optimization history for the volume function considering three different ϵ_v values - column structure with $\overline{\lambda} = 1.2$.

Regarding the buckling moving limit parameter ϵ_b, it has been seen that each topology

optimization problem requires a specific value for this variable, which is dependent on the loading magnitude, geometry properties, etc. This value is defined based on numerical experience, meaning that different move limits are tested until the proper convergence is obtained. For this example, it has been tested different values of ϵ_b and some conclusions were observed. Taking into account that the standard parameter adopted was $\epsilon_b = 1 \cdot 10^{-7}$, if a close value is considered, e.g. $\epsilon_b = 2.5 \cdot 10^{-7}$, the same final design is obtained with little or no influence over the convergence process. On the other hand, if a significant variation is adopted - $\epsilon_b \leq 1 \cdot 10^{-8}$ or $\epsilon_b \geq 1 \cdot 10^{-6}$ -, the solver cannot obtain a feasible integer solution due unsuitable moves of the stability constraint towards the lower limit.

As previously explained, the linearized optimization problem requires small changes between iterations in order to control the truncation error and enable the proper Taylor's series approximation. For this matter, the β variable is usually set to values $\leq 10\%$. As a standard value, this parameter is defined as $\beta = 5\%$ for all the examples solved in this work. In order to observe its influence on the optimization mechanism, two different values were employed in the column-like $\overline{\lambda} = 1.2$ model: $\beta = 2\%$ and $\beta = 10\%$. Such analysis showed that no change was observed for the proposed example, neither for the final solution nor the optimization development. This can be explained for the nature of the optimization problem: both objective function and buckling constraint seeks to prevent the volume reduction in order to present a stiffer and more stable performances, respectively. Therefore, the formulation itself prevents significant changes between iterations and the flip-limits variable does not actively limit this process for this case. On the contrary, optimization problems whose objective function seeks to minimize the structure volume or its thermal expansion, for example, would benefit for a great element change and, thus, the β parameter is effective to avoid this consequence.

5.2.2 Example 2

- **A1 - The fixed pressure case**

The design problem for the fixed fluid-structure boundary is shown in Fig. 20 (a). The volume constraint defines a final fraction of 0.40 of the full design domain. Different buckling constraints ($\overline{\lambda}$) have been defined seeking to investigate the buckling influence on the final topology. As a baseline solution, the conventional optimization set up - compliance minimization under volume constraint - is shown in Figure 20 (b) - and presents a buckling load factor of 0.89. Based on that, the algorithm has been solved for buckling constraints of 1.00 and 1.20. The optimized topologies are shown in Figure 20 (c)-(d).

As expected, the arch-shaped design is obtained for the compliance solution, Fig. 20 (b), and modest design changes are seen as the buckling constraint increases, Fig. 20 (c)-(d). A trade-off between stiffness and stability parameters is commonly observed in buckling-constrained topology optimization problems: the more stable, the less stiff is the final solution [14, 100]. However, Fig. 20 (c) presents a slightly stiffer solution when a higher buckling constraint is assigned for the dry arch problem. This phenomenon can be explained due to the nature of the binary method: the design changes between iterations is not as smooth as seen in density-based variables and, thus, a better local minima solution in terms of stiffness might occur even when a more stable performance is demanded. The expected trend still occurs, seen that for $\overline{\lambda} = 1.20$,

(a) Design problem

(b) $\overline{\lambda} = 0$
($\lambda_1 = 0.89, \quad C = 6.92 \cdot 10^{-4}$)

(c) $\overline{\lambda} = 1.00$
($\lambda_1 = 1.00, \quad C = 6.89 \cdot 10^{-4}$)

(d) $\overline{\lambda} = 1.20$
($\lambda_1 = 1.20, \quad C = 6.93 \cdot 10^{-4}$)
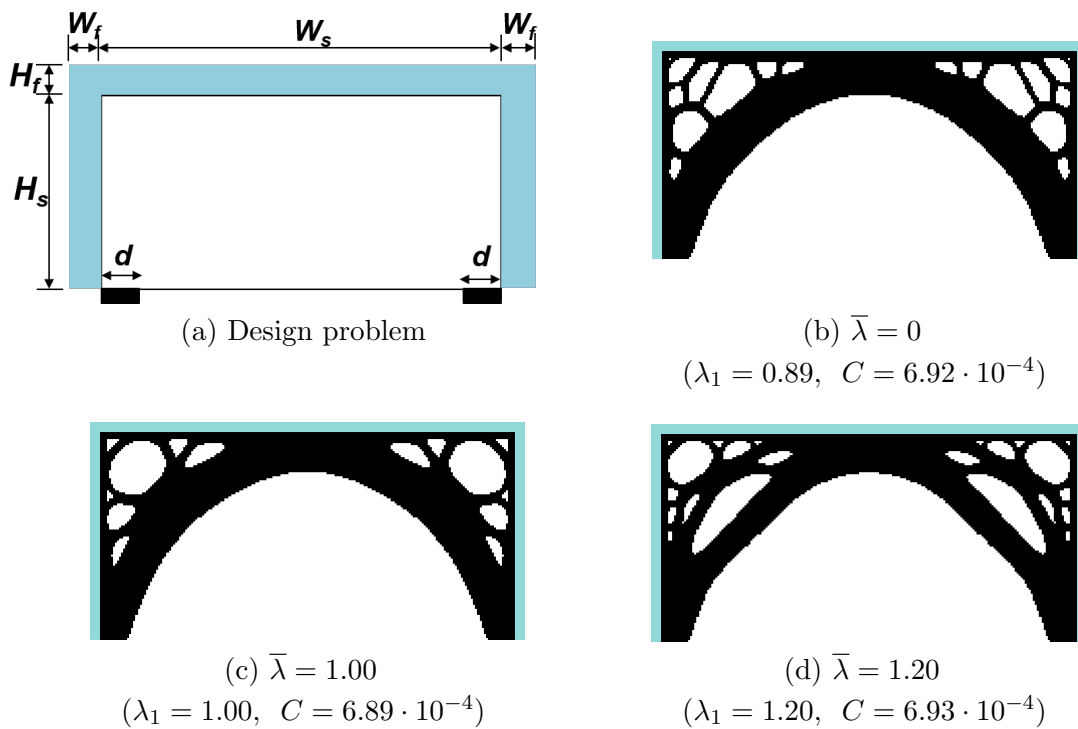
Figure 20: Results compilation of Example 2 - Dry model (A1).

Fig. 20 (c), the compliance is the highest value of the problem ($C = 6.93 \cdot 10^{-4}$)), but this cannot be taken as rule as observed in most of the discussions of density-based works. Still, we advocate that they are similar minima, as the difference in the compliance values between them is quite small.

- **A2 - The design-dependent pressure case**

For this problem, the boundary is able to change between iterations and the fluid pressure loading interacts differently based on the structure design. The optimum design for the classical approach - compliance minimization under volume constraint - was set to a 0.32 final volume fraction, and presents an arch-like topology shown in Figure 21(b); its lowest buckling load factor is 0.94. Then, the problem has been solved for the proposed methodology adopting increasing buckling constraints - as seen in Fig. 21.

In this problem, the full initial solid domain progresses into material removal seeking to satisfy the volume constraint. The elements are free to change from solid to fluid state, changing the fluid-solid interface location and characterizing a design-dependent application problem. Since the TOBS method is adopted, the structure interface is clearly defined due to the binary design variables - a significant advantage when dealing with pressure loading problems.

For the buckling constraint $\overline{\lambda} = 1.4$, Figure 22 shows the optimization history for the compliance and volume functions. As proposed by the TOBS method, the initial domain is defined by a full-solid state, surrounded by the fluid pressure loading. This context expresses a situation where both constraints are distant from their targets, allowing the first iterations to characterize a significant material removing, and impacting to reduce the stiffness and the stability parameters (Fig. 23). Around iteration 80, the lower bound for the stability parameter

(a) $\overline{\lambda} = 0$
($\lambda_1 = 0.94$, $C = 5.63 \cdot 10^{-4}$)

(b) $\overline{\lambda} = 1.20$
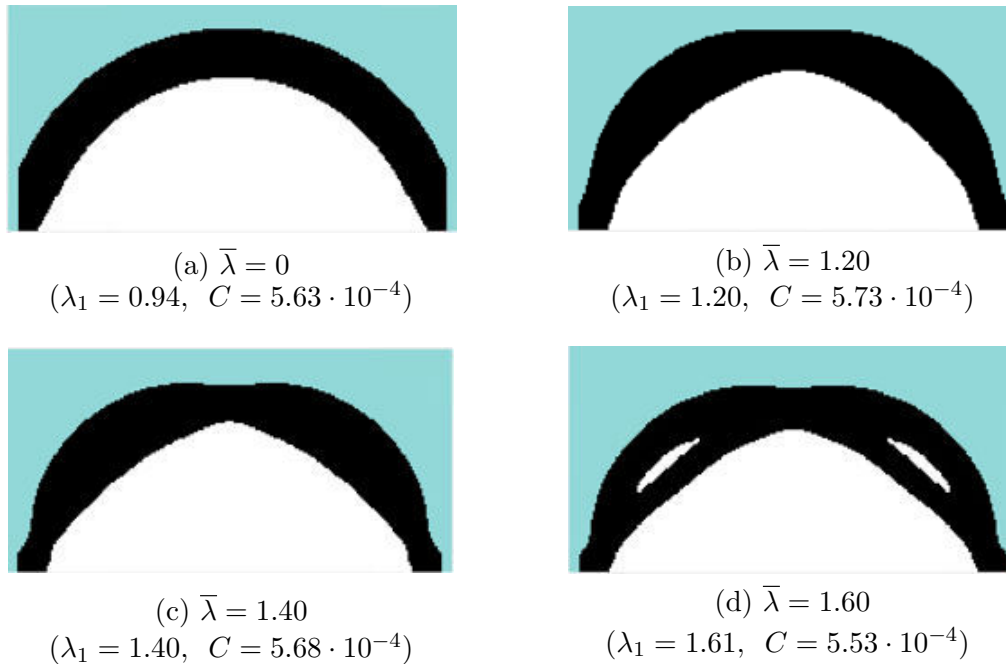($\lambda_1 = 1.20$, $C = 5.73 \cdot 10^{-4}$)

(c) $\overline{\lambda} = 1.40$
($\lambda_1 = 1.40$, $C = 5.68 \cdot 10^{-4}$)

(d) $\overline{\lambda} = 1.60$
($\lambda_1 = 1.61$, $C = 5.53 \cdot 10^{-4}$)

Figure 21: Results compilation of Example 2 - Wet model (A2).

is reached ($\lambda_1 = \overline{\lambda} = 1.6$). The material removal continues, because the volume constraint has not been fulfilled yet, but at a lower pace. The optimizer manages to keep the lowest buckling factor until the moment when the volume constraint constraint is satisfied - around iteration 235. The topology at this point shows two inner holes at the critical regions for the first buckling mode - as shown in Fig. 23 - but the optimizer cannot achieve the convergence right away. Instead, it returns to the arch-like solution, by dissolving the inner holes, and that is the moment where the buckling load factor reaches its lowest value (around 0.7 at iteration 310). Figure 23 also demonstrates that this problem defines a bimodal eigenvalue phenomenon, since both 1st and 2nd buckling modes present close values. In the final optimization stage, the design gets thickened at the critical solutions until it is split, obtaining the final and converged solution.

As discussed for the dry-arch case (A1), the binary method might justify the unexpected behavior of lower compliance values for stiffer solutions. The wet case brings an additional factor that acts on the overall stability-stiffness trade-off: the design-dependent load. As the structure boundary changes throughout the optimization, the fluid-structure interaction is also modified and might create a condition for a stiffer design – in other words, creating different load problems. This also explains why the most stable design, Fig. 21 (d), is also stiffer when compared to the compliance solution Fig. 21 (a).

This example defines a benchmark for design-dependent problems and the arch-fashioned shape has proven to be the stiffest solution [109, 110]. Once the stability constraint is added to the optimization problem, it gradually changes the arch-like solution - see Fig. 21 (b)-(f). It is observed that as the buckling constraint increases, the optimizer thickens the center part of each half side, until a split occurs and creates a void region inside the structure. Thus, the main contribution of this analysis is that modest changes in the layout might enhance the overall stability performance with little or no stiffness sacrifice. This phenomenon can be understood
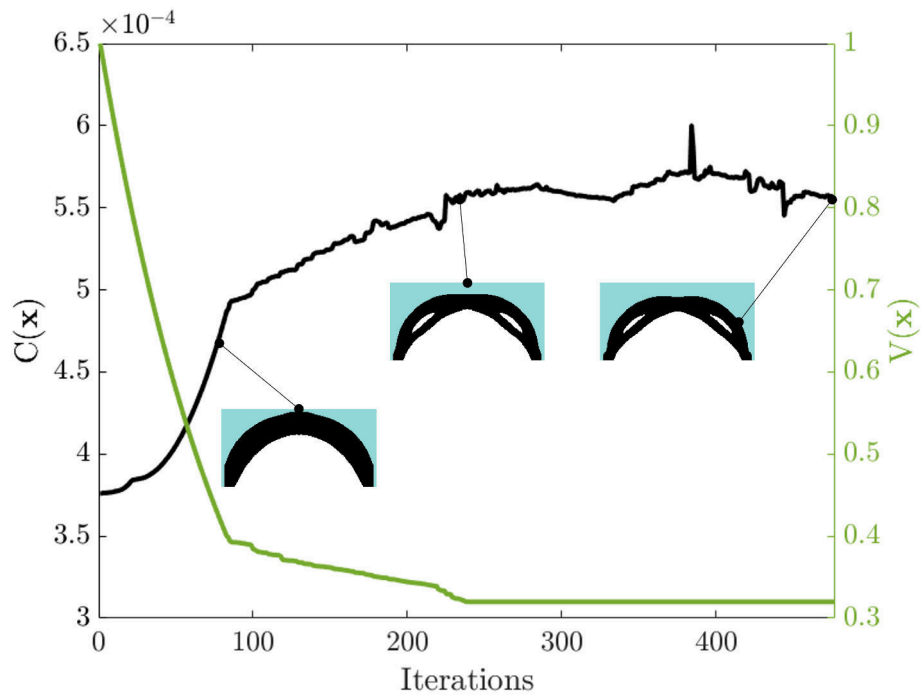
Figure 22: Optimization history for the compliance and volume functions - wet arch with $\overline{\lambda} = 1.6$.
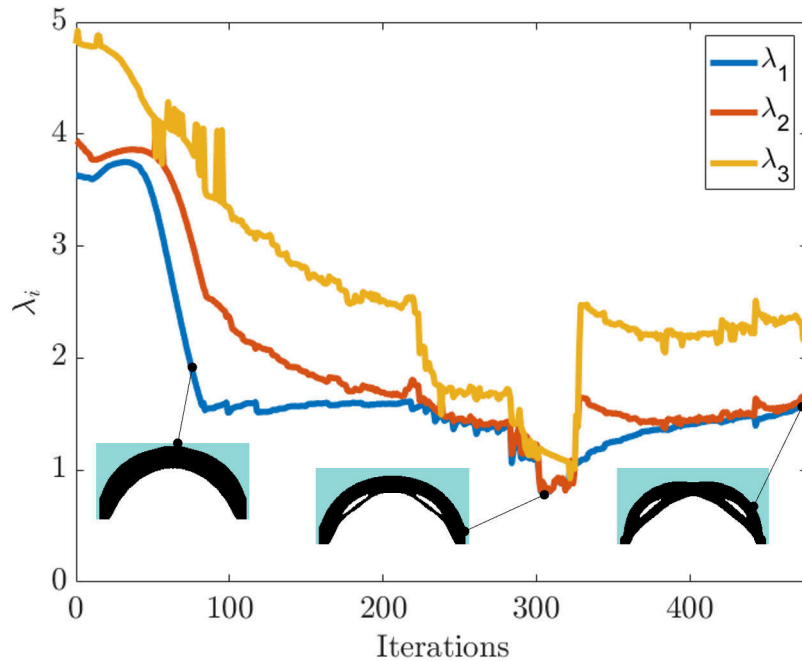
Figure 23: Optimization history for the first three buckling load factors - wet arch with $\overline{\lambda} = 1.6$.

once the first buckling mode is observed for the arch-like design, Fig. 24.

By analysing the first buckling mode for the compliance design, Figure 24 (a) demonstrates that the largest deformations occur at the same regions where the optimizer focus to reinforce in the buckling solution - see 24 (b) -, obtaining a solution more stable by dividing the structure into two main bars. Based on this strategy, the stability parameter increased by 70%, while the compliance value showed no sacrifice regarding the structure's stiffness.

(a) 1st buckling mode – compliance design
$(\overline{\lambda} = 0,\ \lambda_1 = 0.94)$

(b) 1st buckling mode – buckling design
$(\overline{\lambda} = 1.6,\ \lambda_1 = 1.61)$

Figure 24: Comparison of the first buckling mode for the compliance and buckling solutions.

- Mesh-dependency investigation

The novel formulation of the buckling-constrained topology optimization solved by a binary approach brings the discussion on the mesh-dependency. The computed buckling modes have proved to be dependent on the mesh refinement in previous works. For instance, Ferrari and Sigmund (2019) [15] presents some results where localized buckling modes only arise on the finer discretizations. Therefore, in order to briefly comprehend this process on the proposed binary formulation, a coarser and a finer mesh has been considered for the $\overline{\lambda} = 1.4$ buckling-constrained problem. The coarse case is discretized by 106x53 finite elements - Fig. 25 (a), whereas the finest mesh is set to 270x135 (Fig. 25 (b)) - 65% increase in the amount of elements when compared to the standard mesh (210x105), Fig. 25 (c).

(a) 106x53   (b) 210x105   (c) 270x135
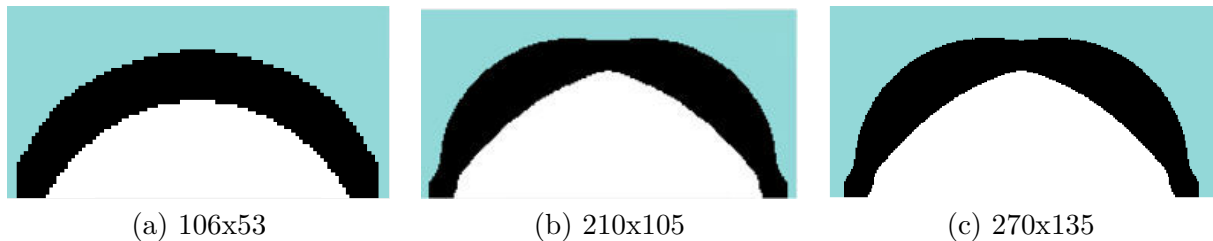
Figure 25: Comparison of three different discretizations for $\overline{\lambda} = 1.4$.

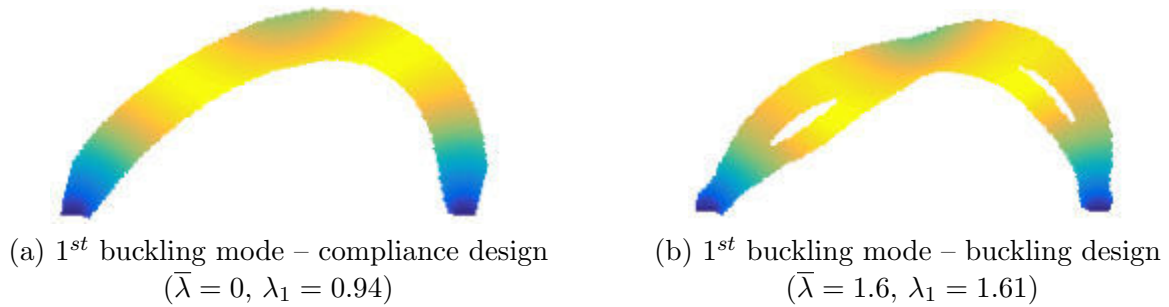Although the coarser mesh maintained the arch-like pattern seen in the compliance design (Fig. 21 (a)), as the mesh got finer, the optimized structure showed the tendency to be mesh-independent. It is seen that different meshes promote a variation in the distribution of the stresses on the structure elements and, thus, might generate different buckling behaviors and final solutions when distinct discretizations are compared [15]. Unfortunately, finer meshes could not be analysed in this problem due to computational limitations. In short, as this is a stress/buckling-based problem, further studies should be developed to obtain a general conclusion about this topic.

5.2.3 Example 3

Another known example from the literature has been studied for the TO considering the buckling mechanism: the piston head model. Two different support conditions were defined seeking to observe its effect on the buckling constraint and the overall optimization convergence.

The first piston-head model is restrained only at the y direction, at the middle node of the bottom edge. The alternative case considers a clamped bottom edge with a width d. Except for the bottom support condition, the same geometry properties are defined for both examples: the design domain is a rectangular area of width $W = 3.00$ and height composed of the solid $H_s = 1.00$ and the fluid $H_f = 0.10$ regions. The domain is divided into 240x88 square elements. The final volume fraction is set as 0.30 for all solutions. A relaxation parameter of $\epsilon_v = 0.005$ is adopted for the volume constraint and $\epsilon_b = 1 \cdot 10^{-8}$ for the stability parameter.

- **V1 - The roller support case**

The design problem is illustrated in Figure 26(a). A constant fluid pressure of $4 \cdot 10^{-4}$ is imposed to the structure. Following the previous methodology, the compliance design has been developed as a reference and a starting point to set the buckling load factor constraints ($\overline{\lambda}$). This final topology is shown in Fig. 26(b), and presents a critical buckling load factor $\lambda_1 = 0.38$. For the proposed approach, the buckling constraint has been set up from 0.8 to 2.0, varying by 0.2. The final designs are compiled in Figure 26.

As seen in Examples 1 and 2, the buckling constraint parameter actively influences on the material distribution and tends to increase the contact points of the structure and the supports. In the piston-head problem, the optimizer reallocates the solid elements from the inner bars to the main parts connected to the side supports, as the buckling lower bound increases - see Fig. 26 (c) - (e). This process causes the decrease of the number and the length of the inner bars that sustain the arch-shaped structure. In order to observe the optimization process for this example, the model with $\overline{\lambda} = 1.20$ - Fig. 26 (e) - has its objective and constraint functions plotted in Figures 27 and 28.

As expected, the compliance increases as the material is removed until the volume constraint is fulfilled (Fig. 27). Figure 28 exhibits an interesting point about the stability performance: the lower lateral bars promote a stable design setting during the early optimization stage, but as the volume decreases and such bars are removed, the three buckling load factors drop drastically around iteration 120. The stability parameter is then controlled and maintain the constraint value until the volume lower bound is reached. This case does not present eigenvalue multiplicity during the final optimization stage, and only the first buckling mode influence its convergence process.

Intuitively, one might think that the slender inner bars are the critical parts of the structure when it comes to stability analysis. On the other hand, when the first three buckling modes are plotted, it is understood the physical meaning of the optimization process based on the deformed shapes - Figure 29.

The first buckling mode demonstrates the way the structure will deform as the lowest buckling load factor is reached. Figure 29(b) shows that the structure as a whole tilts around its bottom support, given the fragile support condition and freedom to move in the x direction. The second buckling mode also composes an overall deformation of the structure, especially at the arc and side edges regions. The inner slender bars become a problem only at the third buckling mode, Fig. 29 (d), not influencing the optimization solution directly. For this case, the bottom support freedom to move at the x direction describes an unstable condition for the problem model and strongly influences the buckling mechanism.

(a) Design problem

(b) $\overline{\lambda} = 0$
$(\lambda_1 = 0.38, \quad C = 9.32 \cdot 10^{-6})$

(c) $\overline{\lambda} = 0.80$
$(\lambda_1 = 0.81, \quad C = 9.61 \cdot 10^{-6})$

(d) $\overline{\lambda} = 1.00$
$(\lambda_1 = 1.00, \quad C = 9.83 \cdot 10^{-6})$

(e) $\overline{\lambda} = 1.20$
$(\lambda_1 = 1.21, \quad C = 9.79 \cdot 10^{-6})$

(f) $\overline{\lambda} = 1.40$
$(\lambda_1 = 1.41, \quad C = 9.91 \cdot 10^{-6})$

(g) $\overline{\lambda} = 1.60$
$(\lambda_1 = 1.63, \quad C = 9.95 \cdot 10^{-6})$

(h) $\overline{\lambda} = 1.80$
$(\lambda_1 = 1.81, \quad C = 9.92 \cdot 10^{-6})$

(i) $\overline{\lambda} = 2.00$
$(\lambda_1 = 2.04, \quad C = 10.06 \cdot 10^{-6})$
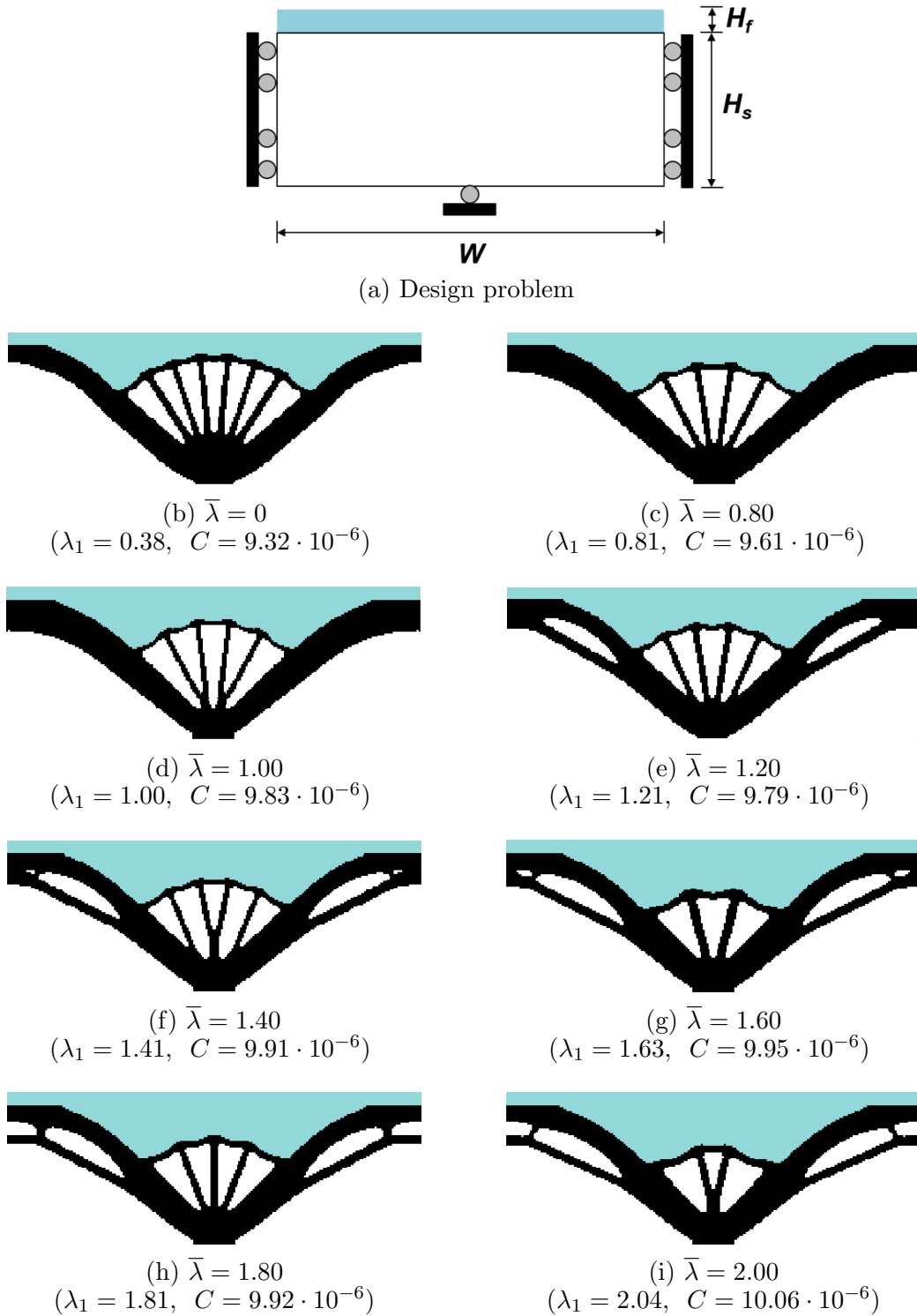
Figure 26: Results compilation of Example 3 - Roller support (V1).

In a practical way, the second and third buckling modes are not critical for this study case because the corresponding buckling load factors are significantly higher than the first mode. Therefore, the solver prioritizes the first mode deformation shape and relocates the material in order to reinforce the main bulky bars and prevent the tilting phenomenon. This example is physically interesting because one might think that the inner slender bars would be the critical parts for the stability analysis. In that context, the linear buckling optimization corroborates
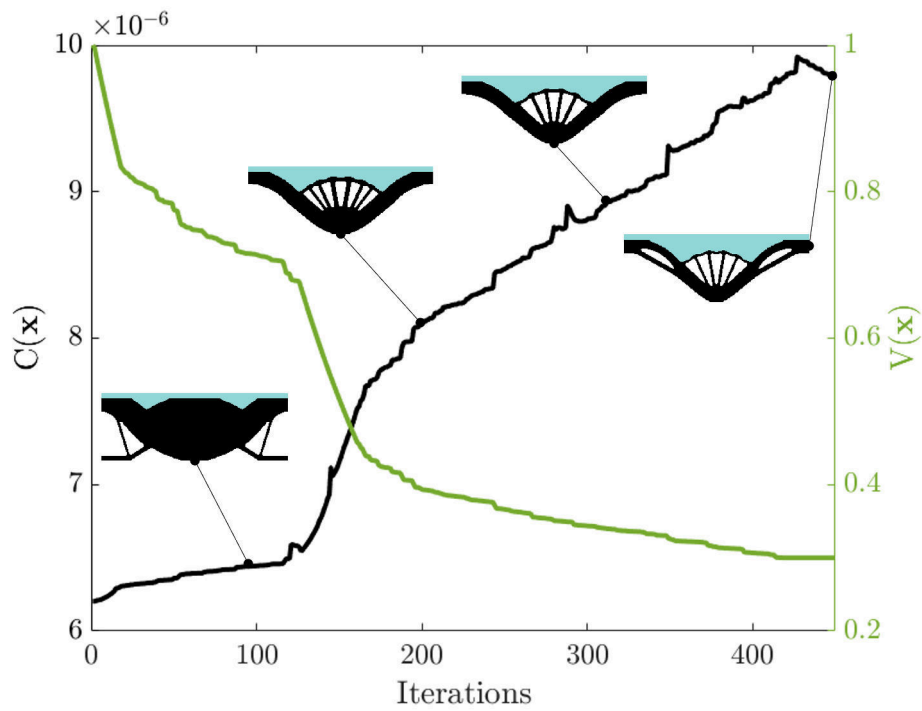
Figure 27: Optimization history for the compliance and volume functions - Piston V1 with $\overline{\lambda} = 1.20$.
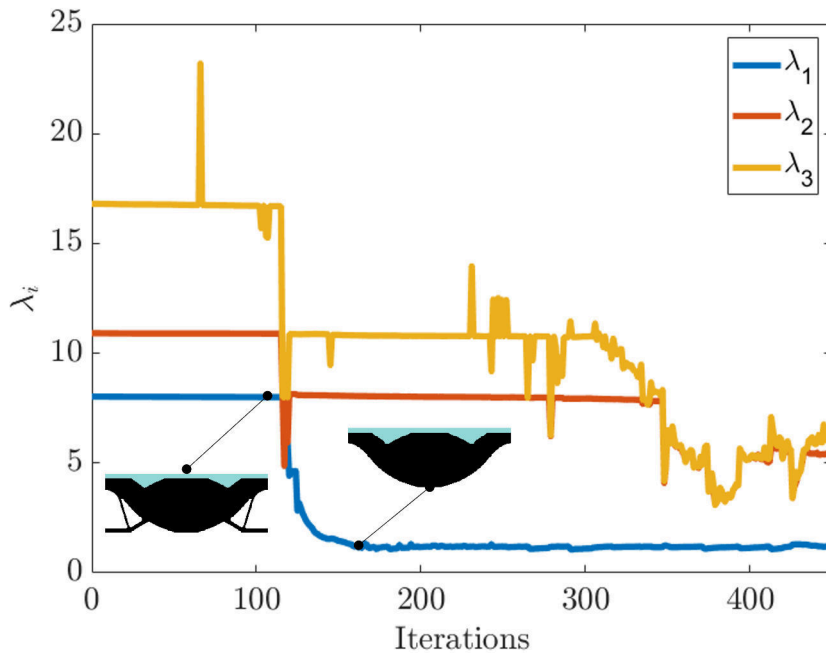
Figure 28: Optimization history for the first three buckling load factors - Piston V1 with $\overline{\lambda} = 1.20$.

the importance of considering this stability parameter as a fundamental design tool.

One fact that proves the efficiency and feasibility regarding the proposed methodology compared to the conventional approach is the overall stability improvement with little compliance increase. Figure 30 demonstrates the difference in percentage of optimized buckling designs compared to the compliance design, regarding the final buckling load factor (λ_1) and final compliance values.

(a) Optimum design for $\overline{\lambda} = 1.2$

(b) 1st Buckling mode ($\lambda_1 = 1.20$)

(c) 2nd Buckling mode ($\lambda_2 = 5.45$)

(d) 3rd Buckling mode ($\lambda_3 = 6.79$)
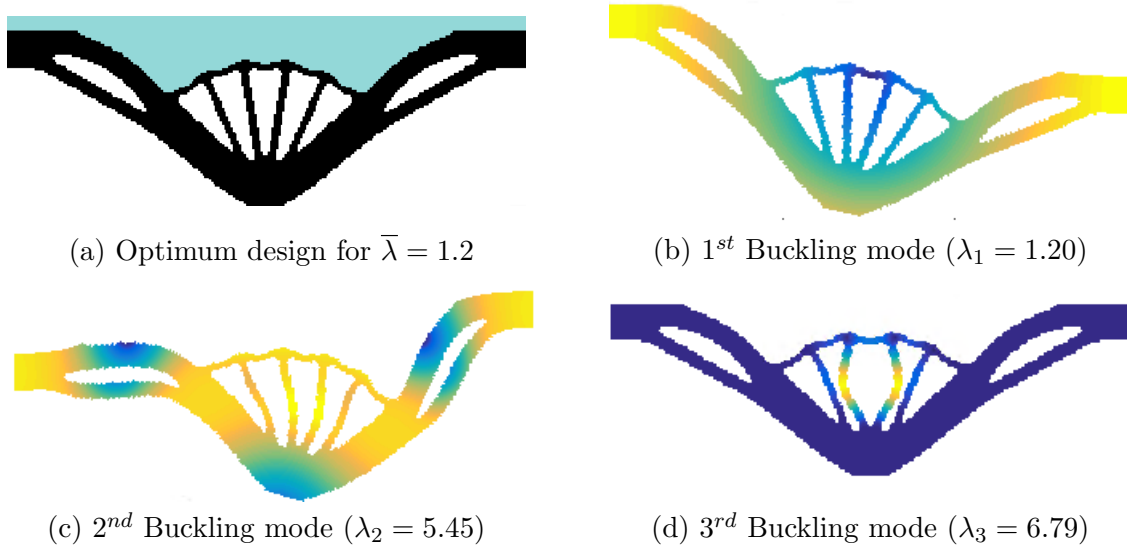
Figure 29: Final topology for $\overline{\lambda} = 1.2$ and its three first buckling modes.
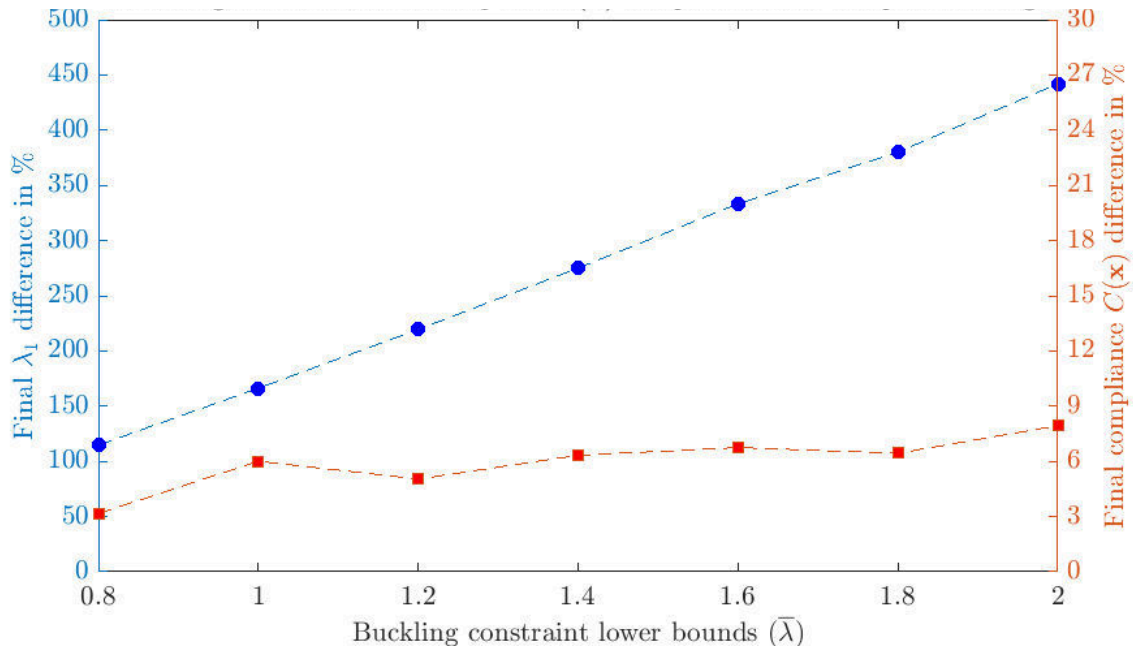
Figure 30: Comparison between buckling models and compliance design of Example 3 - Piston V1.

As seen in Figure 30, for $\overline{\lambda} = 2.0$ design, the final buckling load factor increased in 436% while the compliance got 7.94% higher compared to the compliance baseline design. This scenario corroborates the advantage of considering the stability parameter inside the optimization problem, without compromising the structure's stiffness.

- **V2 - The clamped support case**

As an alternative modeling, the bottom support has been changed for a clamped configuration with width of $d = 0.05$ - see Figure 31 (a). Since this approach composes a case where the structure is more restricted - and intuitively more stable -, a higher pressure load has been defined to obtain similar buckling load factors compared to the point load. Thus, $P = 3 \cdot 10^{-3}$. The compliance design, Fig. 31 (b), presents $\lambda_1 = 0.80$. Thus, the buckling

constraints have been defined from 1.0 to 1.6. The final solutions are shown in Figure 31.

(a) Design problem

(b) $\overline{\lambda} = 0$
($\lambda_1 = 0.80, \quad C = 4.07 \cdot 10^{-4}$)

(c) $\overline{\lambda} = 1.00$
($\lambda_1 = 1.00, \quad C = 4.11 \cdot 10^{-4}$)

(d) $\overline{\lambda} = 1.20$
($\lambda_1 = 1.31, \quad C = 4.16 \cdot 10^{-4}$)

(e) $\overline{\lambda} = 1.40$
($\lambda_1 = 1.40, \quad C = 4.17 \cdot 10^{-4}$)

(f) $\overline{\lambda} = 1.60$
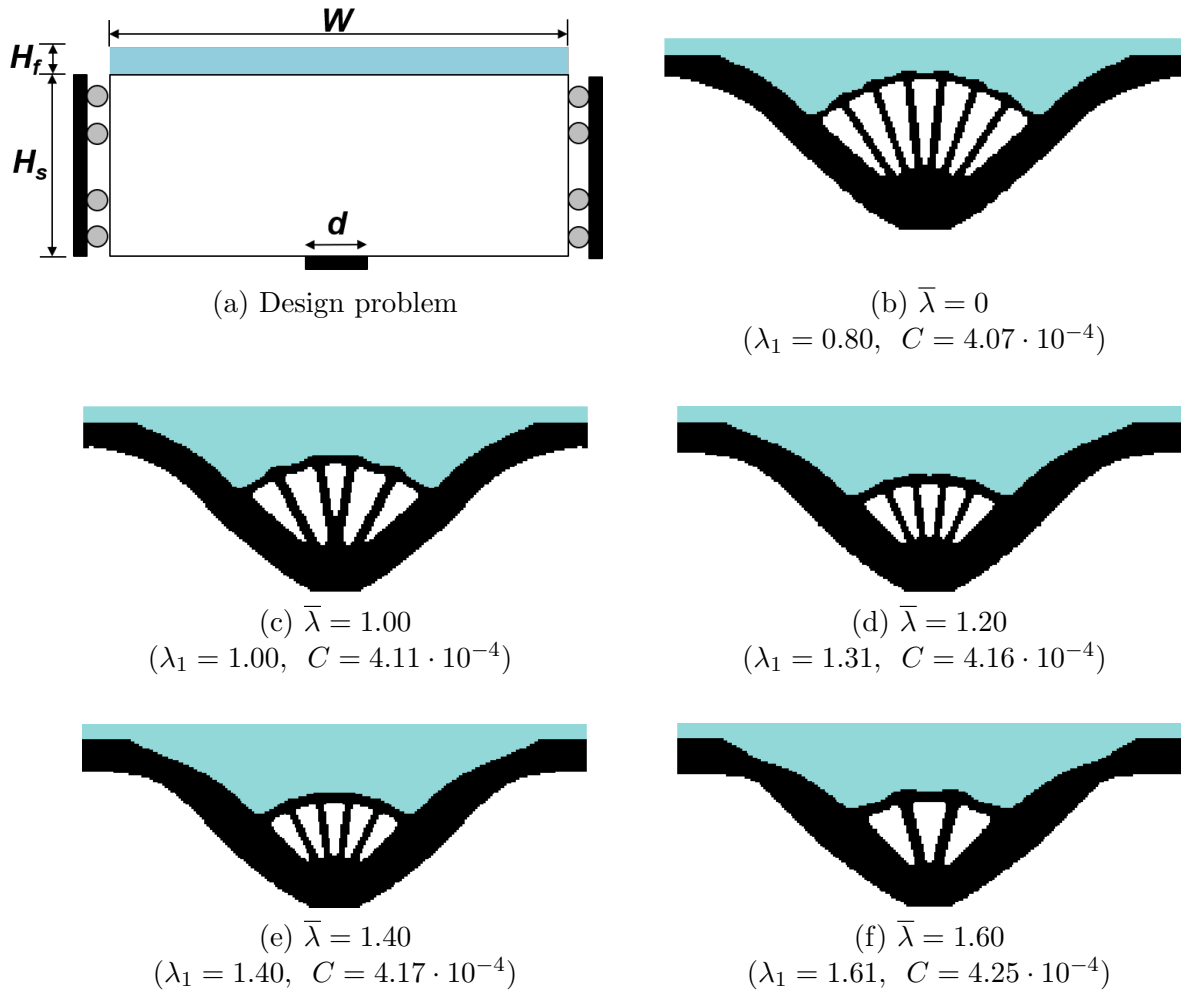($\lambda_1 = 1.61, \quad C = 4.25 \cdot 10^{-4}$)

Figure 31: Results compilation of Example 3 - clamped bottom support.

The compliance design for the clamped support case - Fig. 31 (b) - shows a similar solution when compared to the point support - Fig. 26 (b). This condition demonstrates that, for the stiffness maximization, the change applied on the bottom support does not affect the optimum design. On the other hand, once the buckling constraints are included, a different optimization process is observed. Figure 32 demonstrates the evolution of the compliance and volume values throughout the optimization process, and the intermediate designs. The buckling constraint values are shown in Figure 33, where the first three eigenvalues are plotted for the optimization process. There is a sudden drop in all three buckling load factors at iteration 637, and that occurs due to the smaller lateral inner bars that are about to be disassembled and, thus, a local buckling failure take place for all three buckling modes. This issue is rapidly solved for the next iterations when the values continue a coherent optimization progress until convergence.

It is observed that even presenting a similar design progress when compared to the roller case, the $\overline{\lambda} = 1.2$ clamped model does not create the inner holes near the side support bars and such behavior is explained due to the stability influence. Figure 34 displays first three buckling modes for this model and, when compared to the V1 case (Fig. 29), a new configuration is
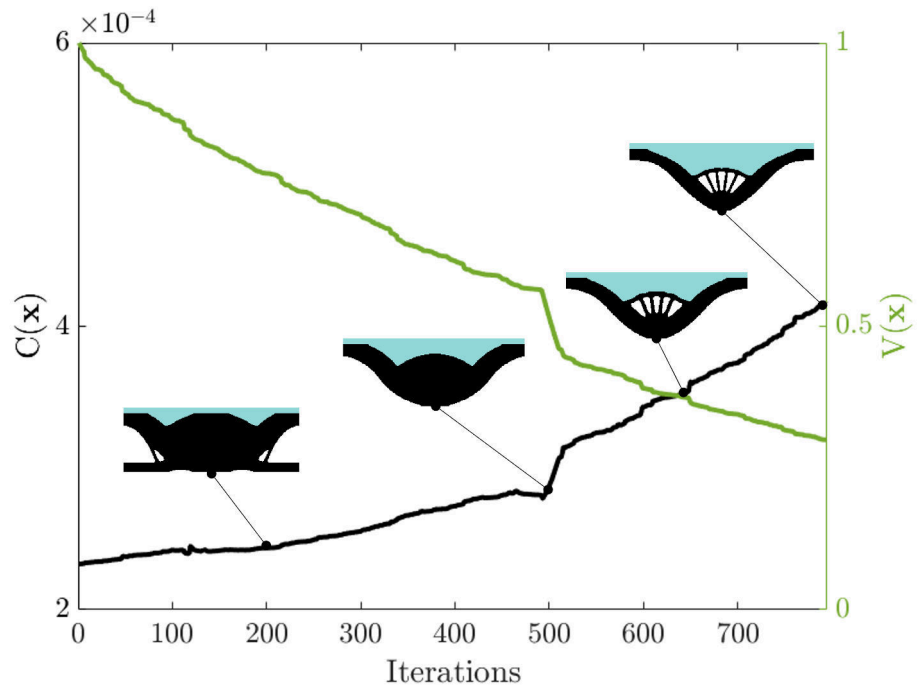
Figure 32: Optimization history for the compliance and volume functions - Piston V2 with $\overline{\lambda} = 1.20$.
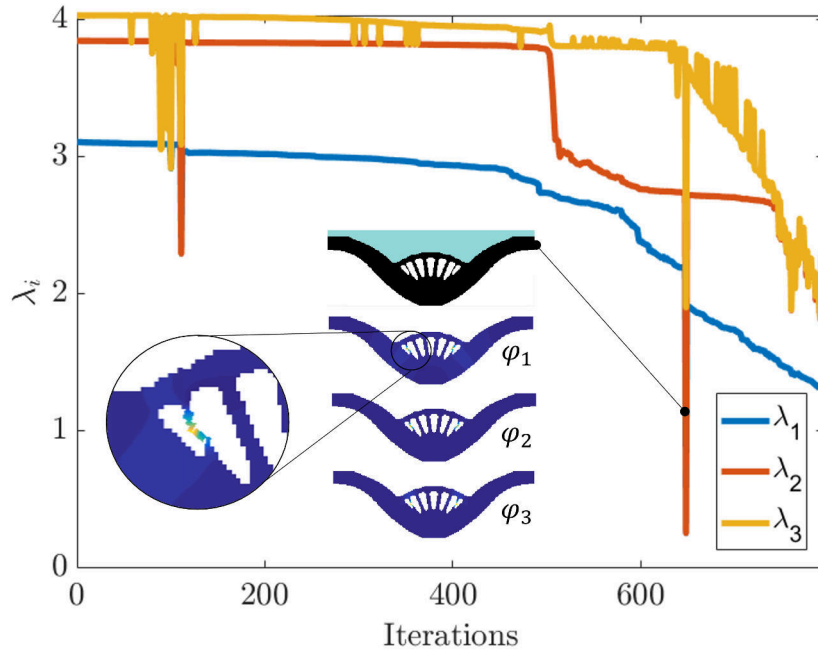
Figure 33: Optimization history for the first three buckling load factors - Piston V2 with $\overline{\lambda} = 1.20$.

achieved. The second and third buckling modes for the weaker support case represent the first and second modes, respectively, for the V2 case. It is assumed, then, that the first buckling mode of the V1 case is directly related to the weaker feature of this bottom support to allow the instability mechanism by its tilting phenomenon. For the current case, the second and third buckling modes correspond to the critical deformation of the inner slender bars. By this analysis, it is seen that as the overall structure becomes more stable - by restricting its support conditions -, the buckling modes related to the overall deformation shift for local modes which

(a) Optimum design for $\overline{\lambda} = 1.2$

(b) 1st Buckling mode ($\lambda_1 = 1.31$)

(c) 2nd Buckling mode ($\lambda_2 = 2.24$)

(d) 3rd Buckling mode ($\lambda_3 = 2.27$)
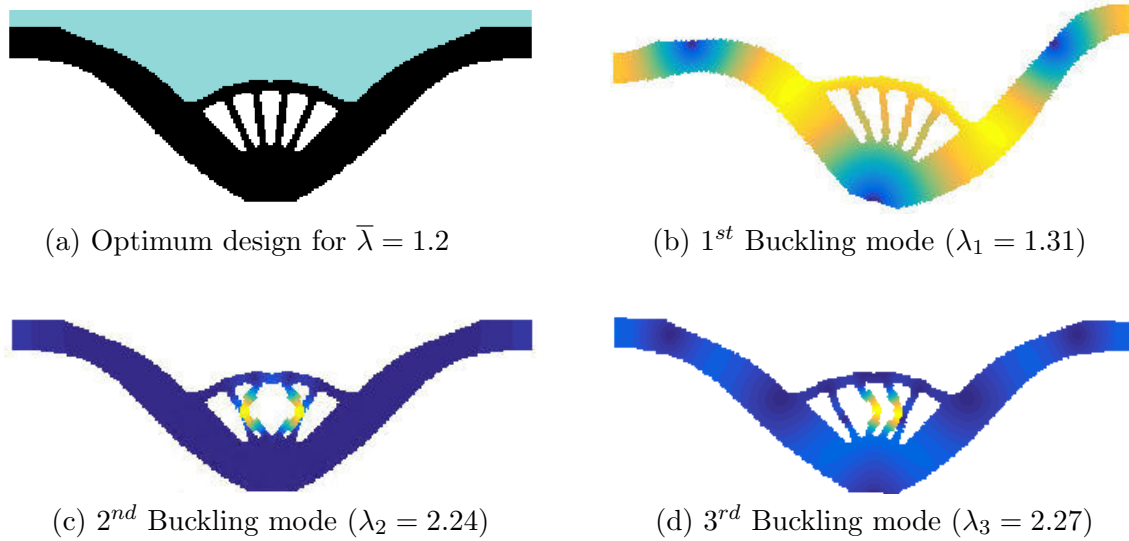
Figure 34: Final topology for $\overline{\lambda} = 1.2$ and its three first buckling modes for the V2 case.

critical members are specific slender parts, such as the inner bars.

- Computational cost analysis

The clamped piston-head model with $\overline{\lambda} = 1.2$ - Fig. 34 (a) - has been optimized via the TOBS method in a total time of 28 hours using a Intel Xeon Silver 4114 - 2x CPU 2.20 GHz - 128GB RAM. The design domain is composed by 21120 elements, and its breakdown times for each optimization step is shown in Figure 35.
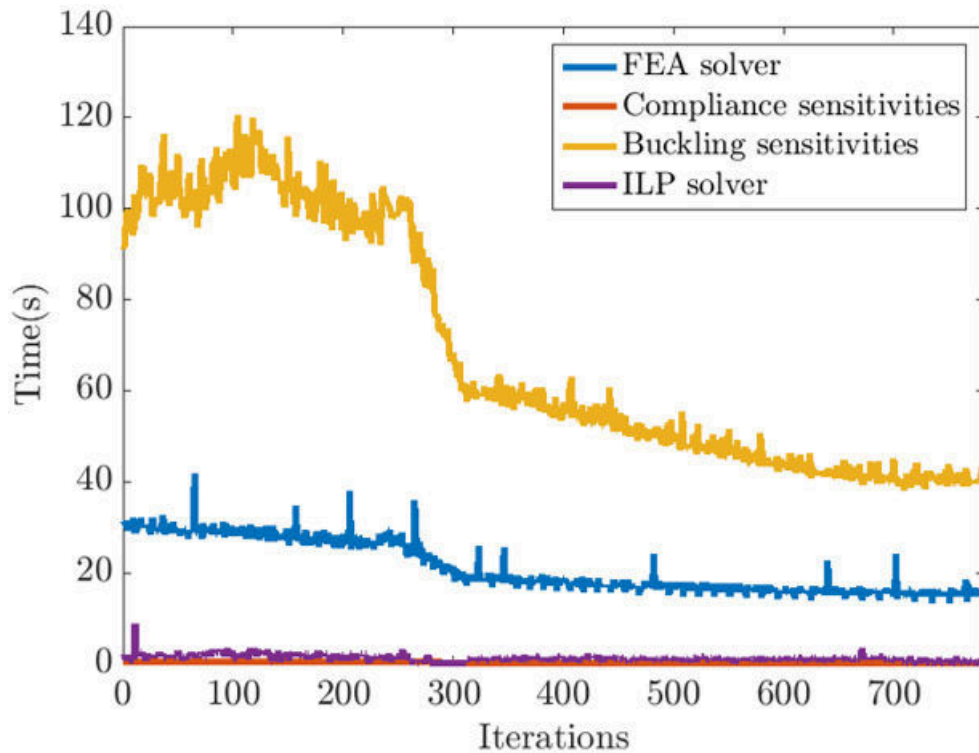
Figure 35: Breakdown computational times for the clamped piston-head $\overline{\lambda} = 1.2$ example with the TOBS method.

It can be seen that the buckling sensitivities required a significant computational time when

compared to the remaining steps. The eigenvalue derivatives took 79.47% out of the entire optimization process. The bottleneck of this process is the adjoint system - Eq. 39 - that is solved for each binary variable and performs implicit displacement derivatives. This scenario expresses a demanding efficiency increase through alternative implementation techniques. It is worth pointing out the the decrease on the computational time throughout the optimization is due to the reduction on the solid regions and, thus, less design variables actively influence the buckling sensitivity analysis.

The Finite Element Analysis solver emerges as a secondary computational effort, representing 18.39% of the total amount of time required to solve the problem. Most of the time consumed for the FEA solver is related to the eigenproblem solution - Eq. 24 - which, this formulation, is computed for the first 20 eigenpairs (λ, φ). This quantity is sufficient to analyse the main critical buckling modes and to avoid unnecessary computational effort for obtaining buckling modes that do not influence over the optimization process.

Despite the unexplored use of integer linear programming, this optimization step is relatively cheap and utilizes less than 2% of the overall time. This fact represents a important feature of the TOBS method, by adopting an optimizer that solves an entire pressure loaded buckling-constrained structure in about one second. Lastly, the compliance sensitivities compose the fastest stage for the optimization and is based on an efficient approach established by Eq. 35, which analytical approach is rapidly computed by the software.

6 CONCLUSIONS

The main contribution of this work is the implementation and investigation of structural topology optimization problems involving stability constraints and design-dependent loading via a binary approach, i.e. the TOBS method. The key findings and developments of this thesis are:

- The linear buckling analysis implementation using FEM has been effectively accomplished and verified through an analytical approach. Its application inside the topology optimization problem as a constraint was also certified based on a benchmark buckling-constrained investigation, i.e. the column-like structure, achieving the meaningful optimum solutions.

- Few examples applied the proposed formulation considering design-dependent loads: the arch-like structure and the piston-head model. The former numerical problem compared the solutions from the fixed and the design-dependent approaches, discussing the particular behavior that the binary method and the loading type combined has on the expected trade-off between stability and stiffness. A brief mesh-dependency verification was investigated and preliminary results have shown the tendency of obtaining solutions that do not depend on the mesh adopted - but further studies are required to reach a general conclusion.

- The piston-head model explored the influence of the support condition on the stability performance and the final optimum solutions. The roller support configuration presented a fragile buckling resistance by leading the stability constraint with a tilting global configuration. The clamped support, on the other hand, showed that a greater movement restriction promotes the criticity of local buckling modes - although the first eigenmode was still related to a global failure setting.

- All numerical examples presented a significant stability improvement when compared to the compliance design, requiring little or no stiffness loss; usually referenced as a common trade-off in the literature [15, 18]. An interesting discussion on this topic is referred to the nature of the proposed formulation in not certainly follow the trade-off rule as seen in previous works. The binary method and the design-dependent loads create the conditions to obtain similar local minima between buckling constraints, and even a lower compliance value for more stable designs, contradicting the trade-off phenomenon.

- The TOBS method effectively solved the numerical examples applying the proposed formulation and avoided common issued related to classical density-based approaches when eigenvalue problems are considered, such as spurious buckling modes, and the need of identifying and tracking the pressure loading surfaces.

6.1 Closing remarks and future work

In short, it is observed the potential to consider this methodology in practical real case problems, dealing with pressure loaded structures that are susceptible to structural collapse, e.g. offshore industry. As a plan of future studies, there are many different investigations to

deepen the application of TO problem formulations, model and solve more complex engineering systems and improve its computational effectiveness. Among the available research topics, it is worth suggesting

- to implement three-dimensional models, exploring the stability parameter influence on such structures;

- to increase the formulation complexity by considering non-linear approaches and geometric imperfections, defining a more robust optimization setting;

- to include different physics inside the optimization problem, e.g. soil-structure interaction modeling seabed influence over the optimum structure solutions or thermal expansion for oil structural systems;

- to investigate the efficiency of different buckling constraint methods , e.g. aggregation functions, seeking to reduce the computational effort required to solve this optimization step.

REFERENCES

[1] S J van den Boom. Topology optimisation including buckling analysis. Master's thesis, Delft University of Technology, 2014.

[2] R. Picelli, A. Neofytou, and H Alicia Kim. Topology optimization for design-dependent hydrostatic pressure loading via the level-set method. *Structural and Multidisciplinary Optimization*, 07 2019.

[3] O Sigmund and P M Clausen. Topology optimization using a mixed formulation: An alternative way to solve pressure load problems. *Computer Methods in Applied Mechanics and Engineering*, 196:1874–1889, 2007.

[4] R Sivapuram and R Picelli. Topology design of binary structures subjected to design-dependent thermal expansion and fluid pressure loads. *Structural and Multidisciplinary Optimization*, 2020.

[5] A G M Michell. The limits of economy of material in frame structures. *Philosophical Magazine*, 8(6):589–597, 1904.

[6] Raphael T Haftka and Zafer Gürdal. *Elements of structural optimization*, volume 11. Springer Science & Business Media, 2012.

[7] R Picelli. *Evolutionary Topology Optimization of Fluid-structure Interaction Problems*. PhD thesis, University of Campinas (Unicamp), 2015.

[8] R. Picelli, Raghavendra Sivapuram, and Yi Xie. A 101-line matlab code for topology optimization using binary variables and integer programming. 08 2020.

[9] Christian Rye Thomsen, Fengwen Wang, and Ole Sigmund. Buckling strength topology optimization of 2d periodic materials based on linearized bifurcation analysis. *Computer Methods in Applied Mechanics and Engineering*, 339:115–136, 2018.

[10] Makoto Ohsaki and Kiyohiro Ikeda. *Stability and Optimization of Structures: Generalized Sensitivity Analysis*. Springer London, 01 2007.

[11] Quantian Luo and Liyong Tong. Elimination of the effects of low density elements in topology optimization of buckling structures. *International Journal of Computational Methods*, 13(06):1650041, 2016.

[12] Quoc Hoan Doan, Dongkyu Lee, Jaehong Lee, and Joowon Kang. Design of buckling constrained multiphase material structures using continuum topology optimization. *Meccanica*, 54, 06 2019.

[13] René Borst, Mike Crisfield, Joris Remmers, and Clemens Verhoosel. Non-linear finite element analysis of solids and structures: Second edition. *Non-Linear Finite Element Analysis of Solids and Structures: Second Edition*, 07 2012.

[14] Federico Ferrari and Ole Sigmund. Revisiting topology optimization with buckling constraints. *Structural and Multidisciplinary Optimization*, 59(5):1401–1415, 2019.

[15] Federico Ferrari and Ole Sigmund. Towards solving large-scale topology optimization problems with buckling constraints at the cost of linear analyses. *Computer Methods in Applied Mechanics and Engineering*, 363:112911, May 2020.

[16] Federico Ferrari, Ole Sigmund, and James K. Guest. Topology optimization with linearized buckling criteria in 250 lines of matlab. *Structural and Multidisciplinary Optimization*, 2021.

[17] F Ferrari and O Sigmund. Revisiting topology optimization with buckling constraints. *Structural and Multidisciplinary Optimization*, (59):1401–1415, 2019.

[18] X Gao and H Ma. Topology optimization of continuum structures under buckling constraints. *Computers and Structures*, (157):142–152, 2015.

[19] Cox S and McCarthy C. The shape of the tallest column. *Math Anal*, (29):547–554, 1998.

[20] Armand J and Lodier B. Optimum design of bending elements. *Int J Number Methods Eng*, (13):373:384, 1978.

[21] Achtziger W. Local stability of trusses in the context of topology optimization, part i: exact modelling. *Struc Optim*, (17):235:246, 1999.

[22] Xiang Bian and Zongde Fang. Large-scale buckling-constrained topology optimization based on assembly-free finite element analysis. *Advances in Mechanical Engineering*, 9:168781401771542, 09 2017.

[23] Miguel Matos Neves, Ole Sigmund, and Martin Bendsøe. Topology optimization of periodic microstructures with a penalization of highly localized buckling modes. *International Journal for Numerical Methods in Engineering*, 54:809 – 834, 04 2002.

[24] Shiguang Deng and Krishnan Suresh. Topology optimization under thermo-elastic buckling. *Struct. Multidiscip. Optim.*, 55(5):1759–1772, May 2017.

[25] Lazarus H. Tenek and Hagiwara Ichiro. Eigenfrequency maximization of plates by optimization of topology using homogenization and mathematical programming. *JSME International Journal, Series C: Dynamics, Control, Robotics, Design and Menufacturing*, 37(4):667–677, February 1994.

[26] P. Browne, C. Budd, N. Gould, H Alicia Kim, and Jennifer Scott. A fast method for binary programming using first-order derivatives, with application to topology optimization with buckling constraints. *International Journal for Numerical Methods in Engineering*, 92:1026–1043, 12 2012.

[27] X. Huang and Yi Xie. Bidirectional evolutionary topology optimization for structures with geometrical and material nonlinearities. *AIAA Journal*, 45:308–313, 12 2006.

[28] Peter Dunning, Evgueni Ovtchinnikov, Jennifer Scott, and H Alicia Kim. Level-set topology optimization with many linear buckling constraints using an efficient and robust eigensolver. *International Journal for Numerical Methods in Engineering*, 107:n/a–n/a, 09 2016.

[29] R Picelli, R van Dijk, W M Vicente, R Pavanello, M Langelaar, and F van Keulen. Topology optimization for submerged buoyant structures. *Engineering Optimization*, online:1–21, 2016.

[30] R Sivapuram and R Picelli. Topology optimization of binary structures using integer linear programming. *Finite Elements in Analysis and Design*, 139:49–61, 2018.

[31] R Picelli, S Ranjbarzadeh, R Sivapuram, R S Gioria, and E C N Silva. Topology optimization of binary structures under design-dependent fluid-structure interaction loads. *Structural and Multidisciplinary Optimization*, 62:2101–2116, 2020.

[32] R Sivapuram and R Picelli. Topology design of binary structures subjected to design-dependent thermal expansion and fluid pressure loads. *Structural and Multidisciplinary Optimization*, 61:1877–1895, 2020.

[33] Raghavendra Sivapuram, Renato Picelli, Gil Ho Yoon, and Bing Yi. On the design of multimaterial structural topologies using integer programming. *Computer Methods in Applied Mechanics and Engineering*, 384:114000, 2021.

[34] P. Browne. Topology optimization of linear elastic structures. 2013.

[35] Konstantinos Chatzis. La réception de la statique graphique en france durant le dernier tiers du xixe siècle. *Revue d'histoire des mathématiques*, 10(1):7–43, 2004.

[36] Hans A Eschenauer and Niels Olhoff. Topology optimization of continuum structures: A review*. *Applied Mechanics Reviews*, 54(4):331–390, 07 2001.

[37] J D Deaton and R V Grandhi. A survey of structural and multidisciplinary continuum topology optimization: post 2000. *Structural and Multidisciplinary Optimization*, 49:1–38, 2014.

[38] M P Bendsoe and O Sigmund. *Topology Optimization - Theory, Methods and Applications.* Springer Verlag, Berlin Heidelberg, 2003.

[39] G.I.N. Rozvany and W. Prager. Optimal design of partially discretized grillages. *Journal of the Mechanics and Physics of Solids*, 24(2):125–136, 1976.

[40] M P Bendsoe and N Kikuchi. Generating optimal topologies in structural design using a homogenization method. *Computer Methods in Applied Mechanics and Engineering*, 71:197–224, 1988.

[41] J T Pereira, E A Fancello, and C S Barcellos. Topology optimization of continuum structures with material failure constraints. *Structural and Multidisciplinary Optimization*, 26(1):50–66, 2004.

[42] M Bruggi. On an alternative approach to stress constraints relaxation in topology optimization. *Structural and Multidisciplinary Optimization*, 36:125–141, 2008.

[43] A Gersborg-Hansen, M P Bendsoe, and O Sigmund. Topology optimization of heat conduction problems using the finite volume method. *Structural and Multidisciplinary Optimization*, 31(4):251–259, 2006.

[44] Shiwei Zhou and Qing Li. Computational design of microstructural composites with tailored thermal conductivity. *Numerical Heat Transfer, Part A: Applications*, 54(7):686–708, 2008.

[45] Bin Wang, Jun Yan, and Gengdong Cheng. Optimal structure design with low thermal directional expansion and high stiffness. *Engineering Optimization*, 43(6):581–595, 2011.

[46] Y M Xie and G P Steven. A simple evolutionary procedure for structural optimization. *Computer and Structures*, 49:885–896, 1993.

[47] Y M Xie and G P Steven. *Evolutionary Structural Optimization.* London: Springer, London, 1997.

[48] O M Querin and G P Steven. Evolutionary structural optimisation using a bidirectional algorithm. *Engineering Computations*, 15:1031–1048, 1998.

[49] X Y Yang, Y M Xie, and G P Steven. Evolutionary methods for topology optimisation of continuous structures with design dependent loads. *Computers and Structures*, 83:956–963, 2005.

[50] X Huang and Y M Xie. Evolutionary topology optimization of continuum structures including design-dependent self-weight loads. *Finite Elements in Analysis and Design*, 47:942–948, 2011.

[51] Michiel Schellekens, Shiwei Zhou, Joseph Cadman, Wei Li, Richard Appleyard, and Qing Li. Design optimization of scaffold microstructures using wall shear stress criterion towards regulated flow-induced erosion. *Journal of biomechanical engineering*, 133:081008, 08 2011.

[52] Raghavendra Sivapuram, R. Picelli, and Yi Xie. Topology optimization of binary microstructures involving various non-volume constraints. *Computational Materials Science*, 154:405–425, 08 2018.

[53] R. Picelli. On the topology optimization of fluid-structure interaction problems with binary design variables. presented at 14th WCSMO, 2021.

[54] J.A. Sethian and Andreas Wiegmann. Structural boundary design via level set and immersed interface methods. *Journal of Computational Physics*, 163(2):489–528, 2000.

[55] M Y Wang, X Wang, and D Guo. A level set method for structural topology optimization. *Computer Methods in Applied Mechanics and Engineering*, 192(1-2):227–246, 2003.

[56] G Allaire and F Jouve. Minimum stress optimal design with the level set method. *Engineering Analysis with Boundary Elements*, 32:909–918, 2008.

[57] X Guo, W S Zhang, M Y Wang, and P Wei. Stress-related topology optimization via level set approach. *Computer Methods in Applied Mechanics and Engineering*, 200:3439–3452, 2011.

[58] Q Xia and M Y Wang. Topology optimization of thermoelastic structures using level set method. *Computational Mechanics*, 42:837–857, 2008.

[59] Zhen Luo, Liyong Tong, and Haitao Ma. Shape and topology optimization for electrothermomechanical microactuators using level set methods. *Journal of Computational Physics*, 228:3173–3181, 05 2009.

[60] Vivien Challis and James Guest. Level set topology optimization of fluids in stokes flow. *International Journal for Numerical Methods in Engineering*, 79, 09 2009.

[61] G Pingen, M Waidmann, A Evgrafov, and K Maute. A parametric level-set approach for topology optimization of flow domains. *Structural and Multidisciplinary Optimization*, 41:117–131, 2010.

[62] Frederic de Gournay, Grégoire Allaire, and François Jouve. Shape and topology optimization of the robust compliance via the level set method. *http://dx.doi.org/10.1051/cocv:2007048*, 14, 01 2008.

[63] Peter Dunning, H Alicia Kim, and Glen Mullineux. Introducing loading uncertainty in topology optimization. *Aiaa Journal - AIAA J*, 49:760–768, 04 2011.

[64] Niels Olhoff and Steen Hjlund Rasmussen. On single and bimodal optimum buckling loads of clamped columns. *International Journal of Solids and Structures*, 13(7):605–614, 1977.

[65] G. Simitses. Optimal vs the stiffened circular plate. *AIAA Journal*, 11:1409–1412, 1973.

[66] Raphael Haftka and Brian Prasad. Optimum structural design with plate bending elements - a survey. *AIAA Journal*, 04 1981.

[67] W. Achtziger. Local stability of trusses in the context of topology optimization part i: Exact modelling. *Structural optimization*, 17:235–246, 1999.

[68] N. S. Khot, V. B. Venkayya, and L. Berke. Optimum structural design with stability constraints. *International Journal for Numerical Methods in Engineering*, 10(5):1097–1114, 1976.

[69] Deaton J and Grandhi R. A survey of structural and multidisciplinary continuum topology optimization: post 2000. *Struc Multidisc Optim*, (49):1–38, 2014.

[70] M M Neves, H Rodrigues, and J M Guedes. Generalized topology design of structures with a buckling load criterion. *Struc Optim*, (10):71:78, 1995.

[71] Esben Lindgaard and Jonas Dahl. On compliance and buckling objective functions in topology optimization of snap-through problems. *Structural and Multidisciplinary Optimization*, 47, 03 2013.

[72] Jian Rong, Yi Xie, and X. Yang. Improved method for evolutionary structural optimization against buckling. *Computers Structures - COMPUT STRUCT*, 79:253–263, 01 2001.

[73] M Bruyneel and P Duysinx. Note on topology optmization of continuum structures including self-weight. *Structural and Multidisciplinary Optimization*, 29:245–256, 2005.

[74] J D Deaton and R V Grandhi. Topology optimization of thermal structures with stress constraints. In *54th AIAA/ASME/ASCE/AHS/ASC Structures, Structural Dynamics, and Materials Conference*, page 1466, 2013.

[75] B C Chen and N Kikuchi. Topology optimization with design-dependent loads. *Finite Elements in Analysis and Design*, 37:57–70, 2001.

[76] E Lee and J R R A Martins. Structural topology optimization with design-dependent pressure loads. *Computer Methods in Applied Mechanics and Engineering*, 233-236:40–48, 2012. In press.

[77] G H Yoon, J S Jensen, and O Sigmund. Topology optimization of acoustic-structure problems using a mixed finite element formulation. *International Journal for Numerical Methods In Engineering*, 70:1049–1075, 2007.

[78] G H Yoon. Topology optimization for stationary fluid-structure interaction problems using a new monolithic formulation. *International Journal for Numerical Methods In Engineering*, 82:591–616, 2010.

[79] F Brezzi and M Fortin. *Mixed and Hybrid Finite Element Methods*. Springer, Berlin, 1991.

[80] G Allaire, F Jouve, and A-M Toader. Structural optimization using sensitivity analysis and a level-set method. *Journal of Computational Physics*, 194:363–393, 2004.

[81] X Huang and Y M Xie. Convergent and mesh-independent solutions for the bi-directional evolutionary structural optimization method. *Finite Elements in Analysis and Design*, 43:1039–1049, 2007.

[82] R Picelli, W M Vicente, and R Pavanello. Bi-directional evolutionary structural optimization for design-dependent fluid pressure loading problems. *Engineering Optimization*, 47(10):1324–1342, 2015.

[83] W M Vicente, R Picelli, R Pavanello, and Y M Xie. Topology optimization of frequency responses of fluid-structure interaction systems. *Finite Elements in Analysis and Design*, 98:1–13, 2015.

[84] R Picelli, W M Vicente, R Pavanello, and Y M Xie. Evolutionary topology optimization for natural frequency maximization problems considering acoustic-structure interaction. *Finite Elements in Analysis and Design*, 106:56–64, 2015.

[85] R Picelli, W M Vicente, and R Pavanello. Evolutionary topology optimization for structural compliance minimization considering design-dependent fsi loads. *Finite Elements in Analysis and Design*, 135:44–55, 2017.

[86] R Picelli. Otimização estrutural evolucionária usando malhas hexagonais. Master's thesis, Universidade Estadual de Campinas, 2011.

[87] A. J. G. Schoofs. *Structural Optimization History and State-of-the-Art*, pages 339–345. Springer Netherlands, Dordrecht, 1993.

[88] Charles Oliveira, Luna Steffen, Carlos Vasconcellos, and Pablo Sanchez. Structural topology optimization as a teaching tool in the architecture. 37, 07 2019.

[89] X Huang and Y M Xie. Evolutionary topology optimization of continuum structures with an additional displacement constraint. *Structural and Multidisciplinary Optimization*, 40:409–416, 2010.

[90] A H Land and A G Doig. An automatic method of solving discrete programming problems. *Econometrica*, 28:497–520, 1960.

[91] R Picelli, R Sivapuram, and Y M Xie. A 101-line MATLAB code for topology optimization using binary variables and integer programming. *Structural and Multidisciplinary Optimization*, online, 2020.

[92] R Sivapuram, R Picelli, and Y M Xie. Topology optimization of binary microstructures involving various non-volume constraints. *Computational Materials Science*, 154(405-425), 2018.

[93] Papadrakakis Manolis, Yiannis Tsompanakis, Ernest Hinton, and J. Sienz. Advanced solution methods in topology optimization and shape sensitivity analysis. *Engineering Computations*, 13:57–90, 08 1996.

[94] Fred Keulen, Raphael Haftka, and Na-Hyung Kim. Review of options for structural design sensitivity analysis. part 1: Linear systems. *Computer Methods in Applied Mechanics and Engineering*, 194:3213–3243, 08 2005.

[95] Raphael T Haftka and Zafer Gürdal. *Elements of Structural Optimization*. Kluwer Academic Publishers, 3rd rev. and expanded ed. edition, 1991.

[96] Matthias Firl. Optimal shape design of shell structures. 01 2010.

[97] O C Zienkiewicz and P Bettess. Fluid-structure dynamic interaction and wave forces. an introduction to numerical treatment. *International Journal for Numerical Methods In Engineering*, 13:1–16, 1978.

[98] H J P Morand and R Ohayon. *Fluid Structure Interaction - Applied Numerical Methods*. John Wiley & Sons, Inc., Masson, Paris, 1st edition, 1995.

[99] F Axisa and J Antunes. *Modelling of Mechanical Systems: Fluid-Structure Interaction*. Butterworth-Heinemann, Oxford, UK, 1st edition, 2007.

[100] Xingjun Gao and Haitao Ma. Topology optimization of continuum structures under buckling constraints. *Computers and Structures*, 157:142–152, 06 2015.

[101] H. Rodrigues, J. Guedes, and M. Bendsøe. Necessary conditions for optimal design of structures with a nonsmooth eigenvalue based criterion. *Structural optimization*, 9:52–56, 1995.

[102] HL Ye, Ning Chen, Pei Shao, and Yun Sui. Topological optimization of plate subjected to linear buckling constraints based on independent continuous mapping method. *Applied Mechanics and Materials*, 602-605:139–143, 08 2014.

[103] R J Vanderbei. *Linear Programming: Foundations and Extensions*. Springer US, 4th edition, 2014.

[104] Alexander Seyranian, Erik Lund, and N. Olhoff. Multiple eigenvalues in structural optimization problems. *Structural Optimization*, 8:207–227, 12 1994.

[105] Miguel M. Neves, Ole Sigmund, and Martin P. Bendsøe. Topology optimization of periodic microstructures with a penalization of highly localized buckling modes. *International Journal for Numerical Methods in Engineering*, 54(6):809–834, 2002.

[106] Jianbin Du and Niels Olhoff. Topological design of freely vibrating continuum structures for maximum values of simple and multiple eigenfrequencies and frequency gaps. *Struct. Multidiscip. Optim.*, 34(6):545, December 2007.

[107] Y. M. Xie and G. P. Steven. *Optimization Against Buckling*, pages 79–92. Springer London, London, 1997.

[108] O Sigmund. Morphology-based black and white filters for topology optimization. *Structural and Multidisciplinary Optimization*, 33(4-5):401–424, 2007.

[109] O. Sigmund and P.M. Clausen. Topology optimization using a mixed formulation: An alternative way to solve pressure load problems. *Computer Methods in Applied Mechanics and Engineering*, 196(13):1874 – 1889, 2007.

[110] Matteo Bruggi and Carlo Cinquini. An alternative truly-mixed formulation to solve pressure load problems in topology optimization. *Computer Methods in Applied Mechanics and Engineering*, 198(17):1500 – 1512, 2009.